Article

Cell Reports

Assembly of Peripheral Actomyosin Bundles in Epithelial Cells Is Dependent on the CaMKK2/AMPK Pathway

Graphical Abstract

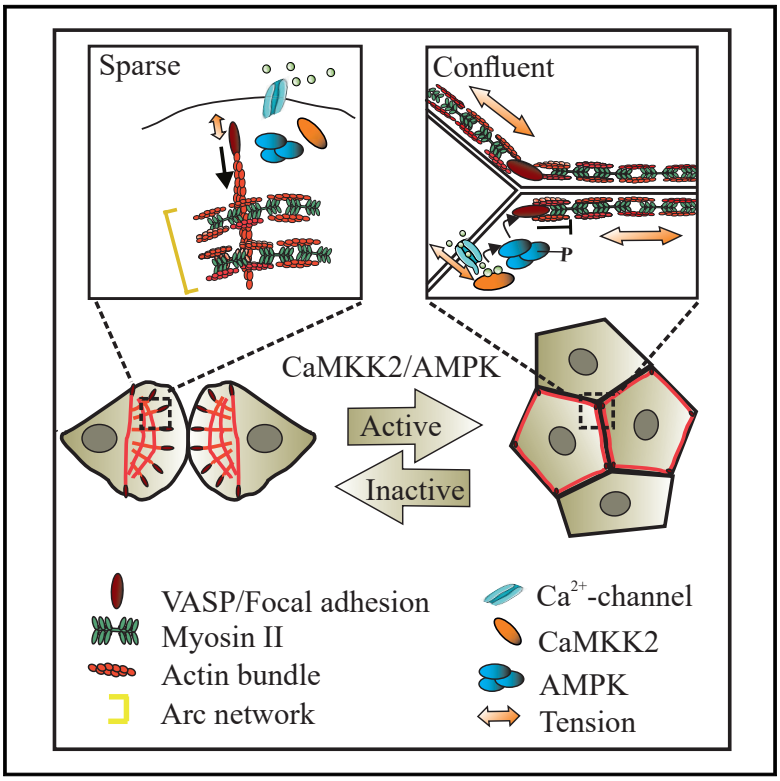

Highlights

- Peripheral actomyosin bundles can be formed from a specific stress fiber subtype
- Maintenance of these bundles is dependent on mechanosensitive CaMKK2/AMPK pathway
- Inhibition of CaMKK2/AMPK pathway leads to redistribution of cellular forces

Authors

Eeva Kaisa Rajakylä, Jaakko I. Lehtimäki, Anna Acheva, Niccole Schaible, Pekka Lappalainen, Ramaswamy Krishnan, Sari Tojkander

Correspondence

sari.tojkander@helsinki.fi

In Brief

Rajakylä et al. show that in epithelial cell cultures, peripheral actomyosin bundles are generated from a specific actin stress fiber type, transverse arcs. Bundle assembly is triggered by a mechanosensitive Ca^{2+}/CaMKK2/AMPK pathway upon cell confluency. Inhibition of this route causes altered cellular force distribution and loss of epithelial cell identity.

Rajakylä et al., 2020, Cell Reports *30*, 4266–4280
March 24, 2020
https://doi.org/10.1016/j.celrep.2020.02.096

CellPress

OPEN ACCESS
CellPress

Cell Reports
Article

Assembly of Peripheral Actomyosin Bundles in Epithelial Cells Is Dependent on the CaMKK2/AMPK Pathway

Eeva Kaisa Rajakylä,[1] Jaakko I. Lehtimäki,[2] Anna Acheva,[1] Niccole Schaible,[3] Pekka Lappalainen,[2] Ramaswamy Krishnan,[3] and Sari Tojkander[1,4,*]
[1]Section of Pathology, Department of Veterinary Biosciences, University of Helsinki, Helsinki, Finland
[2]Institute of Biotechnology, University of Helsinki, Helsinki, Finland
[3]Beth Israel Deaconess Medical Center, Harvard Medical School, Boston, MA, USA
[4]Lead Contact
*Correspondence: sari.tojkander@helsinki.fi
https://doi.org/10.1016/j.celrep.2020.02.096

SUMMARY

Defects in the maintenance of intercellular junctions are associated with loss of epithelial barrier function and consequent pathological conditions, including invasive cancers. Epithelial integrity is dependent on actomyosin bundles at adherens junctions, but the origin of these junctional bundles is incompletely understood. Here we show that peripheral actomyosin bundles can be generated from a specific actin stress fiber subtype, transverse arcs, through their lateral fusion at cell-cell contacts. Importantly, we find that assembly and maintenance of peripheral actomyosin bundles are dependent on the mechanosensitive CaMKK2/AMPK signaling pathway and that inhibition of this route leads to disruption of tension-maintaining actomyosin bundles and re-growth of stress fiber precursors. This results in redistribution of cellular forces, defects in monolayer integrity, and loss of epithelial identity. These data provide evidence that the mechanosensitive CaMKK2/AMPK pathway is critical for the maintenance of peripheral actomyosin bundles and thus dictates cell-cell junctions through cellular force distribution.

INTRODUCTION

Epithelial tissues cover all the surfaces and cavities in animals and provide a selective barrier to enclose functionally distinct units. In epithelial sheets, polarized epithelial cells are anchored and sealed together through a junctional complex, composed of adherens junctions (AJs), desmosomes, and tight junctions (TJs) (Marchiando et al., 2010; Takeichi, 2014). Of these junction types, AJs harbor contractile actomyosin bundles that provide tension to support the junctions (Green et al., 2010; Wu et al., 2014; Lecuit and Yap, 2015). Contractility at AJs is crucial during morphogenesis but also in maintaining normal epithelial homeostasis at post-morphogenetic state (Lecuit et al., 2011; Kannan and Tang 2015; Mason et al., 2016; Curran et al., 2017). During the formation of AJs, small adhesive puncta, connected to radial actin bundles, are initially detected in cells that come in close contact with one another. This initial cell-cell engagement is mediated by cadherins (Yap et al., 1997; Adams et al., 1998), and subsequently several downstream signaling pathways are triggered, leading to spatiotemporal induction of specific Rho-GTPases and recruitment of actin-regulating proteins, such as Arp2/3, N-WASP, Dia1, and Ena/VASP, to stimulate junction assembly (Yamada et al., 2005; Kovacs et al., 2011; Vasioukhin et al., 2000; Acharya et al., 2017). Additionally, E-cadherin ligation recruits myosin II to the cell-cell contacts, and myosin II-produced tension promotes further accumulation of cadherins at the cell junctions (Shewan et al., 2005; Miyake et al., 2006; Yamada and Nelson, 2007; Priya and Yap, 2015). Eventually, the initial adhesive puncta mature into cell-cell junctions that are underlined by peripheral actomyosin bundles, running parallel to the cell edges (Adams and Nelson, 1998; Mège et al., 2006; Meng and Takeichi, 2009; Braga, 2016; Yano et al., 2017). Forces mediated by these actomyosin structures play a crucial role in the maturation of AJs, and interfering with contractility hence drastically affects the formation and stabilization of intercellular junctions (Shewan et al., 2005; de Rooij, 2014; Lecuit and Yap, 2015; Priya and Yap, 2015).

Epithelial cell-cell junctions display two spatially distinct actin populations: junctional actin and thin peripheral actomyosin bundles (reviewed by Gomez et al., 2011; Takeichi, 2014; Braga, 2016). Junctional F-actin pool is located beneath the cell membrane and associates with the E-cadherin-based cell-cell adhesions. This pool of actin is very dynamic and modulated by alterations in Rac1, Cdc42, and RhoA activities, triggering downstream signaling cascades that affect actin assembly, for example, through Arp2/3 and formins (Noren et al., 2001; Kovacs et al., 2002; Sahai and Marshall, 2002; Helwani et al., 2004; Irie et al., 2004; Kobielak et al., 2004; Yamada and Nelson, 2007). The less well-studied peripheral actomyosin bundles (also known as circumferential bundles or thin bundles) were reported in the 1980s as tightly packed, contractile filaments running parallel to the cell-cell junctions (Owaribe et al., 1981; Owaribe and Masuda, 1982). Subsequently, several publications showed the existence of myosin II-containing arched filaments in the lamella of the epithelial cells and also their reorganization upon establishment of cadherin-based adhesions (Vaezi et al., 2002; Zhang et al., 2005; Kalaji et al., 2012; reviewed by Mège et al., 2006;

Gomez et al., 2011; Takeichi, 2014). These two distinct actin filament populations can be visually separated in semi-confluent epithelial cell cultures, but upon maturation of the cell-cell contacts, they become indistinguishable and form the cortical actin ring of the polarized epithelial cells. Both junctional actin and peripheral actomyosin bundles play a role in the maintenance and morphology of epithelial sheets: dynamic junctional actin pool mainly stabilizes cadherin-based adhesions at cell-cell contacts, while the contractile, less dynamic peripheral actomyosin bundles are required to maintain the lateral height of polarized epithelial cells. Their regulation by the Rho effectors ROCK I and II was shown to be essential for the maintenance of lateral height, because interfering with the myosin II-dependent contraction of these structures leads to flattened cells and less compact actomyosin bundles (Kalaji et al., 2012). Although there is a wealth of information about the signaling cascades participating in the dynamics of actin-based structures at AJs, the precise mechanism by which the peripheral actomyosin bundles are originally formed is not fully understood. Furthermore, as these structures resemble a subtype of actin stress fibers, ventral stress fibers, of migrating cells, their relationship to these structures of mesenchymal cells should be assessed.

Migrating mesenchymal cells typically display at least three types of actin stress fibers that can be classified according to their protein compositions and connections with focal adhesions (Small et al., 1998; Tojkander et al., 2012). The assembly of these actin stress fiber types has also been extensively studied. Non-contractile dorsal stress fibers are actin filament bundles that are linked to a focal adhesion from their distal end. Dorsal stress fibers are typically present at the leading edge of the cell, and they elongate toward the cell center through VASP and formin-driven actin filament polymerization at the adhesion (Watanabe et al., 1999; Hotulainen and Lappalainen, 2006; Tojkander et al., 2011, 2015; Oakes et al., 2012; Tee et al., 2015). Transverse arcs are thin, contractile actomyosin bundles that form parallel to the leading edge of the cell and undergo retrograde flow toward the cell center together with the elongating dorsal stress fibers (Hotulainen and Lappalainen, 2006; Burnette et al., 2011; Tojkander et al., 2011; Burnette et al., 2014). Ventral stress fibers are thick actomyosin bundles that are usually enriched toward the back of migrating cells. They represent the major force-producing actomyosin bundles of cells and connect to focal adhesions at their both ends to apply forces to the substrate (Tojkander et al., 2015; Soiné et al., 2015). Importantly, ventral stress fibers can be generated from the pre-existing network of dorsal stress fibers and transverse arcs through lateral fusion of this network (Hotulainen and Lappalainen, 2006; Tojkander et al., 2015; Jiu et al., 2019). At least in U2OS osteosarcoma cells, formation of ventral stress fibers is dependent on the local activation of a signaling cascade composed of Ca^{2+} influxes, Ca^{2+}/calmodulin-dependent kinase kinase 2 (CaMKK2), and 5′ AMP-activated protein kinase (AMPK) that leads to an inhibition of actin filament assembly at focal adhesions through phosphorylation of actin polymerization factor VASP on Ser239. In addition to VASP phosphorylation, this pathway is likely to affect also other aspects of actin dynamics and myosin II activity (Tojkander et al., 2015, 2018).

Here we show that peripheral actomyosin bundles can be built from transverse arc-like precursors during the formation of epithelial sheets. The reorganization and lateral fusion of transverse arc-like actomyosin bundles in confluent cultures was associated with tension-sensitive activation of the CaMKK2/AMPK/VASP pathway. Importantly, inhibition of AMPK, its upstream kinase CaMKK2, or mechanosensitive Ca^{2+} channels upstream of CaMKK2 led to re-formation of actin stress fiber precursors, which altered cellular force distribution and junctional integrity. Consequently, this resulted in a mesenchymal phenotype characterized by formation of lamellipodia-like protrusions, loss of epithelial integrity, upregulation of epithelial-mesenchymal transition (EMT) markers, and scattering of cells in three-dimensional (3D) cultures. These data suggest that mechanical cues, sensed by the epithelial cells, trigger the activation of the Ca^{2+}/CaMKK2/AMPK/VASP pathway to ensure the maturation of tension-maintaining actomyosin bundles of epithelial sheets and that inhibition of this pathway can lead to EMT of epithelial cells.

RESULTS

Peripheral Actomyosin Bundles Can Be Generated from Stress Fiber Precursors

Peripheral actomyosin bundles are crucial for the integrity of epithelial tissues. However, the mechanism by which peripheral actomyosin bundles assemble and their possible relationship with the stress fibers of mesenchymal cells are incompletely understood. To elucidate how these actomyosin bundles form during the maturation of epithelial cell-cell adhesions, we imaged the actin-based structures in Madin-Darby canine kidney (MDCK) epithelial and human breast epithelial (MCF10A) cell lines as single cells without contacts to neighboring cells and in increasing confluency (Figure 1A; Figure S1A). Similarly to the migrating mesenchymal cells (Hotulainen and Lappalainen, 2006; Tojkander et al., 2015), the single MDCK and MCF10A cells exhibited transverse arc-like myosin II-containing actin bundles, which underwent retrograde flow (Video S1). However, accompanied by the increase in confluency, these transverse arc-like bundles concentrated to the cell-cell junctions and appeared to undergo packing into thicker peripheral actomyosin bundles (Figure 1A; Figures S1A and S1B).

Live-cell imaging of MDCK cells expressing GFP-actin or a combination of LifeAct-TagGFP2 and LifeAct-mKate probes provided evidence that upon the formation of cell-cell junctions, the retrograde flow of transverse arcs was ceased, and they began to undergo lateral fusion at the periphery of cells. This resulted in the formation of thicker actin bundles at the intercellular junction, and these eventually matured to a straight actin bundle spanning the cell-cell junction (Figure 1B; Figure S1C; Videos S2A–S2C and S3). A similar assembly mechanism was also observed for outer actomyosin cables at the borders of epithelial cell clusters (Figure S1D; Video S4) Together, these data provide evidence that, at least *in vitro*, peripheral actomyosin bundles can be generated from the pre-existing stress fiber network through lateral fusion of transverse arcs (Figure 1C; Videos S2A–S2C and S3).

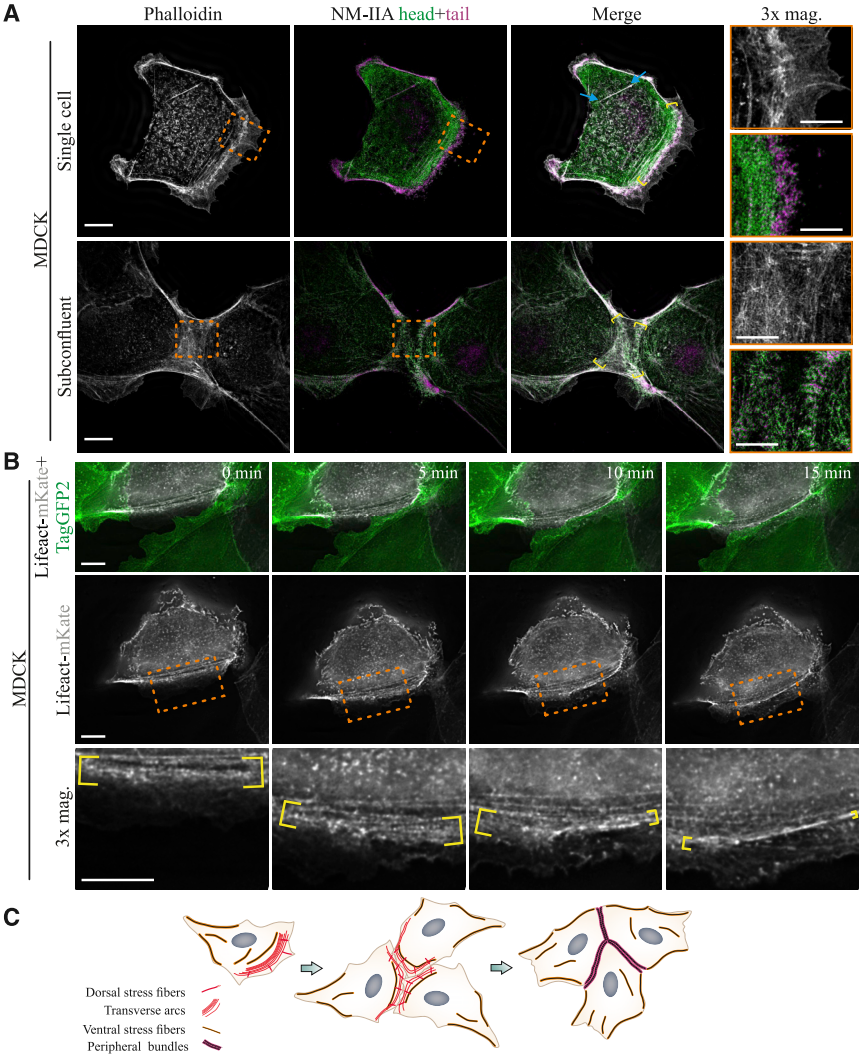

Figure 1. Reorganization of Actin Stress Fiber Network upon Cell-Cell Contact Formation in Epithelial Cell Cultures

(A) 3D-SIM images of representative single and subconfluent MDCK cells stained with anti-myosin light chain-recognizing antibody (detecting NM-IIA motor domains; magenta), antibody against NM-IIA tails (green), and phalloidin (to detect filamentous actin; white). Example of a ventral stress fiber is indicated with blue arrows. Transverse arc networks are indicated with yellow brackets. The 3× magnifications of the indicated areas (orange boxes) demonstrate the presence of bipolar myosin filaments and filament stacks in these structures, both in individual cells and in subconfluent cultures during the cell-cell contact formation. Scale bars, 10 and 5 μm for large images and magnifications, respectively.

(B) Time-lapse imaging of cell-cell contact formation in mixed cultures of MDCK cells expressing either a TagGFP2 or an mKate1.31 fusion of the LifeAct peptide (Videos S2A–S2C). Upper panel shows both TagGFP2 and mKate-LifeAct-expressing cells upon contact formation. Lower panels display only the mKate-LifeAct-expressing MDCK cell, with 3× magnifications of the indicated areas (orange boxes) to illustrate the condensing transverse arc network (yellow brackets). Scale bars, 10 μm.

(C) Schematic representation of the reorganization of actin stress fibers upon increasing confluency.

See also Figure S1.

The Formation of Peripheral Actomyosin Bundles Is Accompanied by the Activation of AMPK/VASP Pathway

Maturation of ventral stress fibers in U2OS osteosarcoma cells depends on the mechanosensitive activation of AMPK/VASP pathway that inhibits elongation of dorsal stress fibers and consequently allows arc fusion (Tojkander et al., 2015). Because formation of peripheral actomyosin bundles resembled the maturation of ventral stress fibers, we examined whether AMPK activation is linked to the assembly of these actomyosin bundles in epithelial cells. For this purpose, cell lysates from both sparsely growing and confluent MCF10A cultures were prepared and analyzed for AMPK activity (Figure 2A). As expected, western blot analysis revealed higher levels of E-cadherin in the confluent cultures compared with the sparse cultures. Interestingly, reaching confluency also led to significantly higher levels of active P-Thr172-AMPK and increased phosphorylation of its downstream target VASP on Ser239 residue (hereafter referred to as P-AMPK and P-VASP, respectively), while the total levels of these proteins remained almost unaltered (Figures 2A and 2B). Moreover, a general increase in AMPK activity was detected with the fluorescence resonance energy transfer (FRET)-based biosensor AMPKAR (Tsou et al., 2011) in confluent MDCK cultures (Figures 2C and 2D; Figures S2A and S2B). Activation of AMPK in confluent epithelial cultures was sensitive to actomyosin-generated tension as inhibition of myosin II by blebbistatin in the confluent monolayer of MCF10A cells led to a significant decrease in the levels of P-VASP (Figures 2E and 2F). These results demonstrate that the formation of peripheral actomyosin bundles from their precursors in epithelial cells coincides with the mechanosensitive activation of the AMPK/VASP pathway.

Inhibition of CaMKK2/AMPK/VASP Pathway in Epithelial Cultures Leads to the Re-appearance of Stress Fiber Precursors

AMPK can be activated by its upstream kinase CaMKK2 in a Ca^{2+}-sensitive manner (Carling, 2017; Hurley et al., 2005; Jensen et al., 2007; Abbott et al., 2009; Tojkander et al., 2018). In migrating U2OS cells, tension can induce CaMKK2-dependent AMPK activation, which is important for the maturation of contractile actin stress fibers (Tojkander et al., 2018). To elucidate the possible role of the CaMKK2/AMPK pathway in the assembly and maintenance of peripheral actomyosin bundles in epithelial monolayers, we used specific inhibitors against CaMKK2 and AMPK (STO-609 and compound c, respectively,

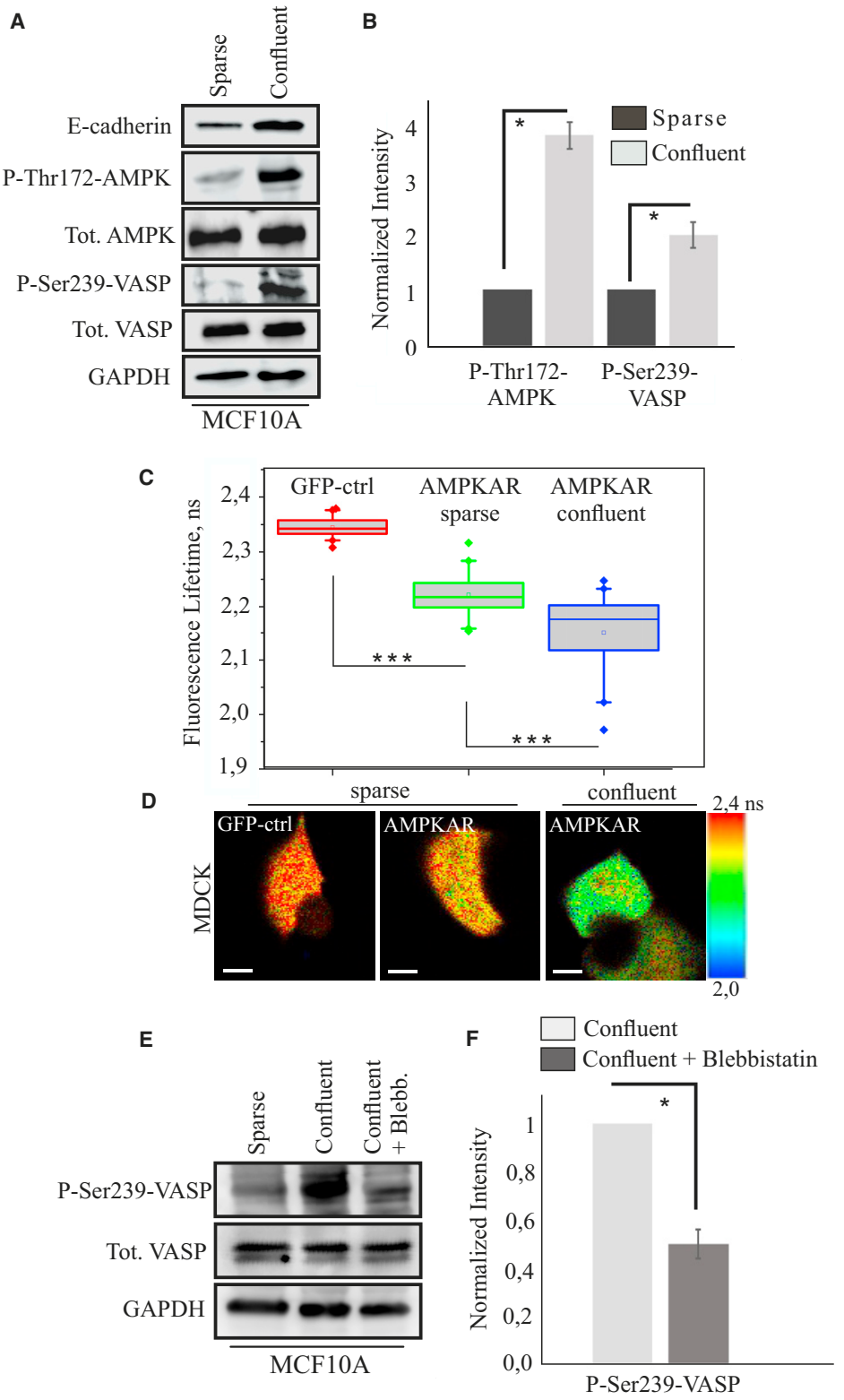

Figure 2. Reorganization of Actin Stress Fibers in Confluent Epithelial Sheets Is Associated with Activation of the AMPK/VASP Pathway

(A) Western blot analysis of cell lysates from sparse and confluent MCF10A cell cultures shows elevated levels of both P-AMPK and P-VASP, while total protein levels remained almost unaltered. Additionally, E-cadherin levels were increased in confluent cell cultures. GAPDH was used as a loading control.

(legend continued on next page)

hereafter referred to as CaMKK2 and AMPK inhibitors) in MDCK and MCF10A cell cultures. Inhibition of either kinase led to subsequent decreases in the levels of P-AMPK and P-VASP in both cell lines, while total protein levels remained almost unaltered (Figures 3A and 3B). Importantly, inhibition of CaMKK2 or AMPK in MDCK monolayer cultures resulted in disruption of peripheral actomyosin bundles and re-appearance of stress fibers with subsequent changes in cell morphology (Figures 3C and 3D). In addition, treatment of MDCK cell clusters with these inhibitors led to loss of outer actomyosin cables surrounding the epithelial islands, as well as re-appearance of multiple focal adhesions, transverse arcs, and dorsal stress fiber-like structures perpendicular to arcs at the newly formed "leading edges" of these cells (Figures 3E–3G; Figure S2C). As Rho-GTPase family members have been strongly associated with the regulation of actin-based structures (Pollard et al., 2000; Arnold et al., 2017), we examined whether inhibition of CaMKK2 or AMPK would affect the activity of the major Rho-GTPAases and in this way the organization of actin cytoskeleton in epithelial sheets. However, by using a Rho-GTPase kinase assay, we revealed that inhibition of the CaMKK2/AMPK pathway did not significantly alter the activity of RhoA, Rac1, or cdc42 (Figures S2D and S2E).

We further used live-cell imaging and fluorescence recovery after photobleaching (FRAP) to detect the dynamics of actin cytoskeleton in control and inhibitor-treated epithelial cell monolayers as well as epithelial cell clusters. These experiments revealed that the outer actomyosin cables, present at the edges of polarized epithelial cell clusters, behaved similarly to the ventral stress fibers of migrating U2OS cells (Tojkander et al., 2015), as these bundles displayed very slow actin polymerization from their focal adhesion-associated ends. In contrast, the dorsal stress fiber-like structures, which replaced the outer actomyosin cables in CaMKK2-inhibited MDCK cells, displayed much more rapid elongation from the focal adhesions (Figures S2F and S2G). Furthermore, live-cell imaging experiments with confluent MDCK monolayers and MDCK cell clusters showed that CaMKK2 or AMPK inhibitor-induced effects on epithelial cell cultures could be reversed by washing out the drug. Thus, re-appearance of the peripheral actomyosin bundles or packing of the outer cables was detected following removal of the inhibitor (Figures S3A, S3B, S4A, and S4B). Together, these data provide evidence that the mechanosensitive CaMKK2/AMPK/VASP pathway regulates the organization of actin filament structures in epithelial cultures and that at least the outer actomyosin cables surrounding the confluent epithelial islands display similar dynamics than the ventral stress fibers of single migrating cells.

To examine the possible role of Ca^{2+} in the activation of CaMKK2, we cultured MCF10A and MDCK cells in a Ca^{2+}-free media for up to 6 h. Expectedly, deprivation of Ca^{2+} from the culture media disrupted the monolayer integrity (Figure S5A). Moreover, Ca^{2+} depletion led to a decrease in the levels of P-AMPK, while the total levels of AMPK remained constant (Figures S5B and S5C). Depletion of Ca^{2+} also diminished the levels of P-Ser19-MLCII and P-Y822-vinculin (hereafter referred to as P-MLC and P-Vinc) (Figures S5B and S5C), indicating a decrease in the junctional tension and correlating with the loss of intact cell-cell borders. This suggests that local Ca^{2+} influxes could activate CaMKK2 at the cell-cell junctions. To assess the possible role of Ca^{2+} channels for the maintenance of epithelial actomyosin bundles, we used GsMTx-4, an inhibitor that targets several mechanosensitive Ca^{2+} channels, including TRP-family channels and Piezo (Sugimoto et al., 2017). Incubation of MDCK cells with this inhibitor led to a loss of both peripheral actomyosin bundles and outer actomyosin cables (Figures S5D–S5F), accompanied by the formation of protrusive structures that contained stress fiber precursors (Figures S5D and S5E). Note that this phenotype was similar to the one resulting from CaMKK2/AMPK/VASP pathway inactivation.

Together, these experiments provide evidence that the mechanosensitive CaMKK2/AMPK/VASP pathway, activated by Ca^{2+} influxes, controls the maturation and maintenance of peripheral actomyosin bundles. Consequently, inactivation of this pathway in epithelial cultures leads to reactivation of VASP and subsequent re-formation of stress fiber precursor structures that normally exist only in migrating cells.

Re-appearance of Stress Fiber Precursors in Confluent Epithelial Cultures Is Associated with Altered Distribution of Cellular Forces

Ventral stress fibers represent the major force-producing structures among the different stress fiber types (Tojkander et al., 2015; Soiné et al., 2015). Because inhibition of CaMKK2/AMPK pathway disrupted the peripheral actomyosin bundles and outer actomyosin cables, which on the basis of our data resemble ventral stress fibers of individual migrating cells, we studied how disruption of this pathway would affect the cell-exerted forces. Polarized MDCK clusters typically possess outer actomyosin cables at the edges of cell clusters. Traction force microscopy analysis revealed that they applied force to the

(B) Quantification of the phosphorylated AMPK and VASP from western blot experiments of sparse and confluent MCF10A cultures. Mean (±SEM) is shown; n = 4 for both P-AMPK and P-VASP. The intensity values were normalized to GAPDH, and values for sparse samples were set to 1. *p < 0.05 (paired t test).
(C) Activity of AMPK in sparse and confluent cultures was detected with AMPKAR biosensor, containing mCherry and GFP tags (see also Figure S2). Single MDCK cells expressing GFP alone or AMPKAR in comparison with confluent AMPKAR-expressing cells were assessed for GFP lifetime (ns) from live-cell imaging experiments. Data are presented as boxplots, where the median is indicated by the central bar. Fifth and 95th percentile whiskers with outliers are shown. n = 24 for all conditions. ***p < 0.001 (Mann-Whitney-Wilcoxon rank-sum test).
(D) Representative examples of fluorescence lifetime (ns) maps of GFP- and AMPKAR-expressing MDCK cells. Scale bars, 20 μm.
(E) Increasing confluency triggers the activation of AMPK/VASP pathway (increases in P-AMPK and P-VASP, respectively) in MCF10A cells. However, treatment of confluent cultures with blebbistatin led to a significant decrease in P-VASP levels. P-VASP and total VASP levels were detected with specific antibodies. GAPDH is shown as a loading control.
(F) Quantification of P-VASP levels from confluent MCF10A cultures treated with solvent only or with blebbistatin. P-VASP levels were divided with corresponding GAPDH values, and values of untreated samples were set to 1.
Mean (±SEM) is shown; n = 3; *p < 0.05 (paired t test).
See also Figure S2.

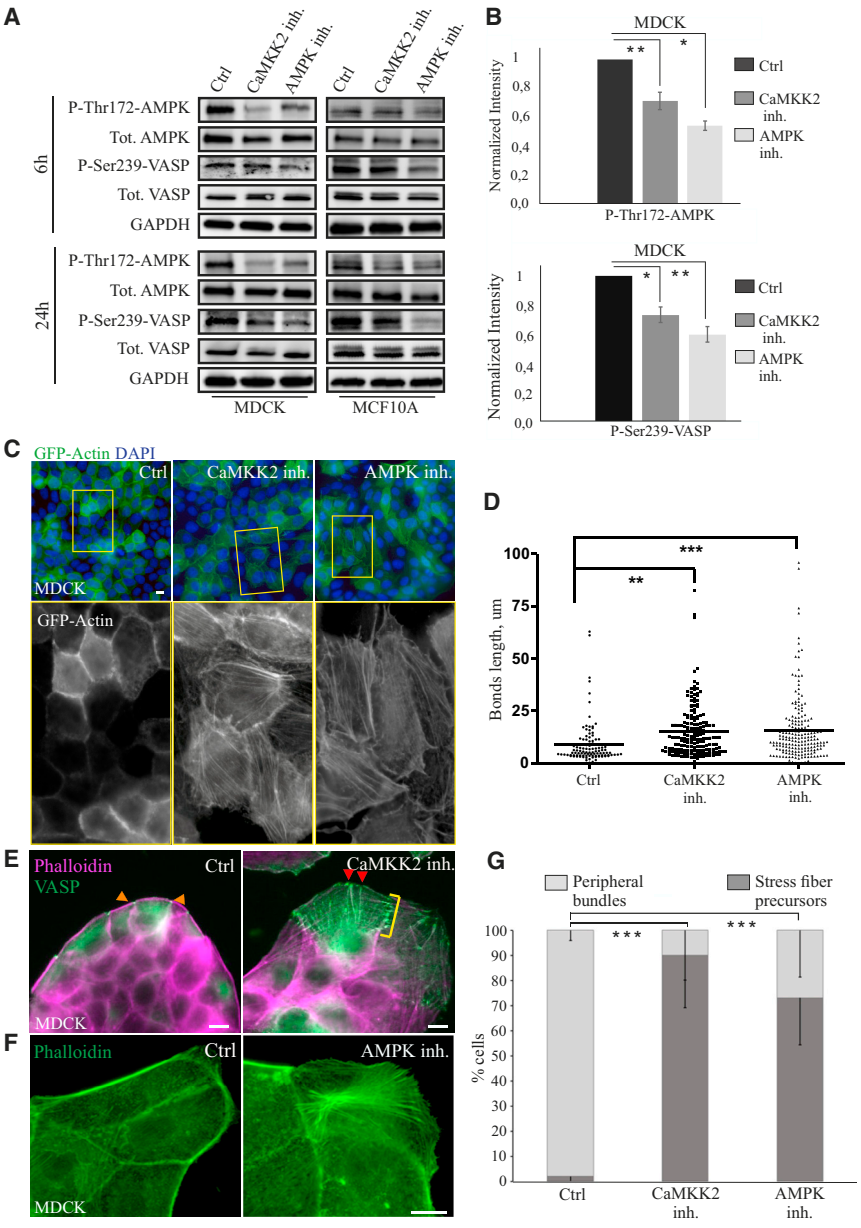

Figure 3. Inhibition of the CaMKK2/AMPK Pathway Leads to Altered Cell Polarity and Restoration of Stress Fiber Precursors

(A) Western blot analysis of lysates from MDCK and MCF10A cells, treated with CaMKK2 or AMPK inhibitors (5 μM STO-609 and 5 μM compound c, respectively) for 6 or 24 h, shows decreased levels of P-AMPK and P-VASP, while the total levels of the proteins remained relatively constant. GAPDH was used as a loading control.

(B) Quantification of P-AMPK and P-VASP protein levels from the western blot data on MDCK cells treated with CaMKK2 or AMPK inhibitors for 24 h. P-AMPK and P-VASP levels were normalized to the corresponding GAPDH values, and control samples were set to 1. *$p < 0.05$ and **$p < 0.01$ (paired t test). Mean (±SEM) is shown; n = 5 for all conditions.

(C) The organization of actin cytoskeleton in a wild-type (Ctrl) GFP-actin-expressing MDCK cell monolayer and monolayers treated with the CaMKK2 or AMPK inhibitors for 16 h. The actin cytoskeletons are visualized with phalloidin (green) and nuclei with DAPI (blue). Magnifications of the indicated areas (yellow boxes) with phalloidin staining are shown below (grayscale images). Scale bar, 20 μm.

(D) Analysis of the cell-to-cell bond lengths in CaMKK2 and AMPK inhibitor-treated monolayers performed with ImageJ plugin Tissue Analyzer. **$p < 0.01$ and ***$p < 0.001$ (one-way ANOVA, Tukey post-test).

(E) The organization of the actin cytoskeleton in the edge of an untreated (Ctrl) MDCK cell cluster and a cluster treated with the CaMKK2 inhibitor for 6 h. CaMKK2 inhibitor-treated cluster undergoes alteration from apicobasal cell shape to a more mesenchymal morphology, accompanied by re-synthesis of stress fiber precursors. The actin filaments were visualized with phalloidin (magenta) and VASP with a specific antibody (green). Orange arrows indicate focal adhesions at the ends of contractile peripheral bundle and red arrows the focal adhesions associated with dorsal stress fibers. Scale bars, 20 μm.

(F) Immunofluorescence images of a wild-type (Ctrl) MDCK cell cluster and a cluster treated with the AMPK inhibitor for 6 h. Phalloidin was applied to visualize the actin cytoskeleton. Scale bars, 20 μm.

(G) Quantification of the percentual amounts of thick peripheral bundles and stress fiber precursors from MDCK cell clusters treated with DMSO (Ctrl), CaMKK2, or AMPK inhibitors for 16 h. n (ctrl) = 214, n (CaMKK2 inhibitor) = 96, and n (AMPK inhibitor) = 127 cells, from two independent experiments.

Mean ± SD is shown. ***$p < 0.001$ (Mann-Whitney-Wilcoxon rank-sum test).

See also Figures S3–S6.

substrate through adhesions associated with the ends of the bundle (Figure S6A, upper panel). Upon inhibition of CaMKK2/AMKP pathway, force distribution was altered as the cells started to resynthesize actin stress fiber precursors. Such cell clusters also displayed a larger number of focal adhesions that exerted tractions at the edges of the clusters (Figure S6A, middle and lower panels). Because both CaMKK2 and AMPK inhibition also caused disruption of the peripheral actomyosin bundles in epithelial monolayers, we examined their effect on forces at cell-cell junctions. For this purpose, LifeAct-mKate-expressing MDCK cell doublets were imaged on traction force imaging dishes (stiffness 6.3 kPa) to monitor bead displacement upon cell-exerted forces. Both tractions as well as intercellular stresses were calculated by using monolayer stress microscopy (Figures 4A and 4B; Figure S6B; Tambe et al., 2011; Feng et al., 2018). Inhibition of the CaMKK2/AMPK pathway reduced the mean values of tractions and the maximum principal normal stress, calculated over the entire doublet as well as in the vicinity of the cell-cell contact (Figures 4A and 4B). Additionally, measuring the monolayer forces from CaMKK2/AMPK-inhibited

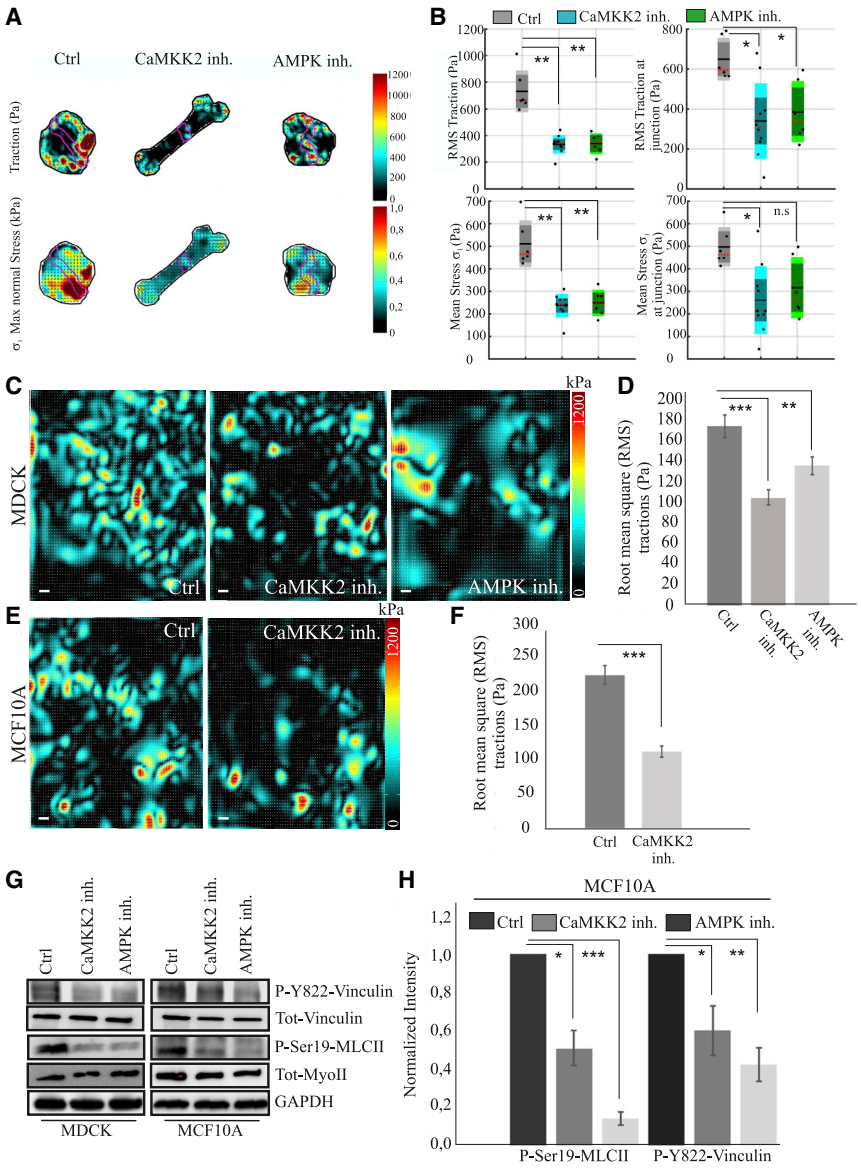

Figure 4. Re-synthesis of Actin Stress Fiber Precursors Is Associated with Altered Force Distribution within Epithelial Cultures

(A) Representative force maps from ctrl, CaMKK2-inhibitor (15 μM STO-609), or AMPK inhibitor (15 μM compound c) treated MDCK doublets after 3 h incubation. Tractions (Pa) are shown in the upper panel and maximal normal stress (kPa) in the lower panel. Cell-junction area is drawn with purple color.

(B) Quantification of the root mean square (RMS) tractions and mean stress in the whole cell or at the cell-cell junctions. Data are presented in boxplots. n (ctrl) = 6, n (CaMKK2 inhibited) = 10, and n (AMPK inhibited) = 6. **p < 0.01 and *p < 0.05; n.s., not significant (Mann-Whitney-Wilcoxon rank-sum test).

(C) Representative examples of monolayer force measurements from untreated (control), CaMKK2-inhibited (16 h), and AMPK-inhibited (16 h) MDCK monolayers. Scale bars, 20 μm.

(D) Quantification of the monolayer forces (monolayer-substrate forces) in untreated (control), CaMKK2-inhibited (16 h), and AMPK-inhibited (16 h) samples. Mean ± SEM is shown; n (ctrl) = 50, n (CaMKK2 inhibited) = 51, n (AMPK inhibited) = 31. **p < 0.01 and ***p < 0.001 (Mann-Whitney-Wilcoxon rank-sum test).

(E) Representative monolayer force maps of untreated MCF10A cells (control) and cells after inhibition of CaMKK2 (16 h). Scale bar, 20 μm.

(F) Quantification of monolayer forces from control and CaMKK2-inhibited MCF10A monolayers (corresponding to E). Mean ± SEM is shown. n (ctrl) = 10, n (CaMKK2 inhibited) = 10. ***p < 0.001 (Mann-Whitney-Wilcoxon rank-sum test).

(G) Western blot analysis of cell lysates from untreated (control), CaMKK2 inhibitor-treated, or AMPK inhibitor-treated MDCK and MCF10A cells 24 h after treatment revealed a decrease in P-MLCII and P-vinculin levels. GAPDH was used as a loading control.

(H) Quantification of P-MLCII and P-vinculin levels from western blot experiments on MCF10A cells (B), normalized against the GAPDH levels. Control values were set to 1. Mean ± SEM is shown. n (P-MLC) = 4, and n (P-vinculin) = 5. *p < 0.05, **p < 0.01, and ***p < 0.001 (paired t test).

See also Figure S7.

cultures revealed that the total cell-substrate forces applied by either MDCK or MCF10A cells were decreased (Figures 4C–4F). Inhibition of CaMKK2 or AMPK pathway, or depletion of Ca^{2+}, also diminished the levels of P-MLC and P-Vinc (Figures 4G and 4H; Figures S5B and S5C), indicating a decrease in junctional tension and loss of integrity of cell-cell contacts. Together, these data provide evidence that inhibition of the CaMKK2/AMPK pathway affects stress fiber assembly in epithelial cells and subsequently leads to redistribution of cellular forces and loss of epithelial integrity due to altered junctional tension.

Activation of AMPK Reinforces the Formation of Epithelial Actomyosin Bundles and Junctional Tension

Because inhibition of the CaMKK2/AMPK pathway led to disruption of both peripheral actomyosin bundles and outer actomyosin cables, we also examined if activation of AMPK would affect the morphology of epithelial cells. For this purpose, we triggered AMPK activity using the chemical compound AICAR in sparsely growing MCF7 breast cancer cells. Single MCF7 cells typically displayed very low AMPK activity and long dorsal stress fibers (Figures 5A and 5B). Interestingly, AICAR treatment resulted in thick actin bundles at the cell periphery, resembling the cytoskeletal organization of confluent epithelial cultures (Figures 5B and 5C). Additionally, activation of AMPK in MDCK monolayer cultures by AICAR increased the intensity of P-Thr18/Ser19-MLCII (PP-MLC) at the cell-cell junctions, as visualized by immunofluorescence microscopy (Figure 5D). Such changes in MDCK monolayers upon AICAR treatment led to increased cell-exerted forces and contractile moment as measured using monolayer force microscopy (Figures 5E and 5F). AICAR treatment further resulted in significant increases in the levels of phosphorylated MLCII and vinculin as detected by western blotting, indicating

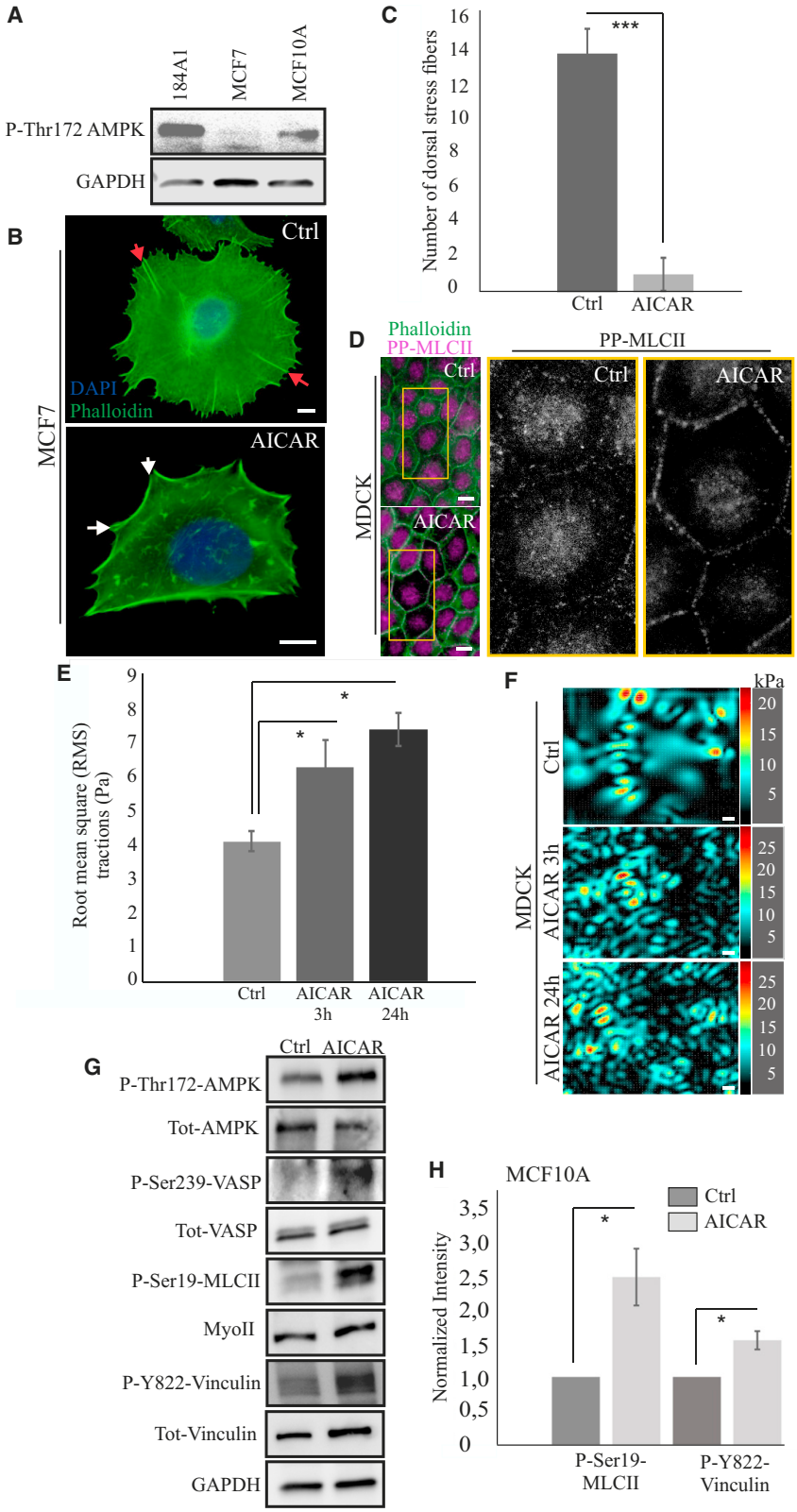

Figure 5. Activation of AMPK Leads to Reorganization of Actin Stress Fibers and Increased Peripheral Tension

(A) MCF7 breast carcinoma cells display very low levels of AMPK activity, as detected by the western blot of lysates from MCF10A, MCF7, and 184A1 cells. P-AMPK was detected with specific antibody. GAPDH was used as a loading control.

(B) Wild-type (Ctrl) MCF7 cells display a large number of dorsal stress fibers (red arrows, upper panel). Reactivation of AMPK by AICAR (25 μM for 16 h) led to a radical reduction of dorsal stress fibers and formation of peripheral bundles (orange arrows, lower panel). Scale bars, 10 μm.

(C) Quantification of the numbers of dorsal stress fibers in control and AICAR-treated MCF7 cells. n (ctrl) = 12 and n (AICAR) = 15 cells. Mean (±SEM) is shown; ***p < 0.001 (Mann-Whitney-Wilcoxon rank-sum test).

(D) Immunofluorescence images of confluent MDCK monolayers that were treated with solvent alone (Ctrl) or with 25 μM AICAR for 16 h. The latter showed more prominent staining of P-Thr18/Ser19-MLCII, as detected with specific antibody (PP-MLCII, magenta) at the cell periphery. Phalloidin was used to visualize actin filaments (green). Magnifications of the indicated areas (yellow boxes) with PP-MLCII staining are shown on the right (grayscale images). Scale bars, 20 μm.

(E) Quantification of monolayer forces from control (solvent) and AICAR-treated (25 μM for 16 h) MDCK cells. Mean ± SEM is shown. n = 5 for all samples. *p < 0.05 (Mann-Whitney-Wilcoxon rank-sum test).

(F) Representative force maps from monolayer traction force experiments of confluent MDCK cells grown on 1 kPa substrates. Scale bars, 20 μm.

(G) Western blot experiments of lysates from control (solvent) and AICAR-treated MCF10A cells showed elevated levels of P-AMPK, P-VASP, P-MLCII, and P-vinculin upon activation of AMPK. GAPDH was used as a loading control.

(H) Quantification of P-MLCII and P-vinculin protein levels from western blots (E). Control values were normalized to 1. Mean (± SEM) is shown. n = 4 for both P-MLCII and P-vinculin. *p < 0.05 (paired t test).

elevated junctional tension (Figures 5G and 5H). These data provide further evidence that activation of AMPK can induce the formation of peripheral actomyosin bundles through reorganization of stress fiber precursors and that formation of actomyosin bundles at the edges of epithelial cells is associated with increasing cell-exerted forces.

Inactivation of the CaMKK2/AMPK Pathway Results in Upregulation of EMT-Associated Factors and Mesenchymal Phenotype

Abnormal AMPK activity is associated with the progression of several invasive cancers, at least through its role in the regulation of central metabolic pathways and cell proliferation (Carling, 2017). Because our experiments provided evidence that inhibition of AMPK and its upstream kinase CaMKK2 can also affect the organization of actin-based structures and distribution of cellular forces in epithelial monolayers (Figures 3, 4, and 5), we examined the cytoskeletal effects of this pathway on EMT and scattering of epithelial cells.

Protrusive activity of the cells was previously shown to contribute to the junctional tension and consequently to the scattering of epithelial cells (Maruthamuthu and Gardel, 2014). To understand whether the loss of junctional integrity after inhibition of CaMKK2/AMPK pathway was due to increased protrusive activity, we used round fibronectin-coated soft (4 kPa) micropatterns to test whether restricted growth area would affect this process. GFP-actin-expressing MDCK cells, treated with solvent alone or with the CaMKK2 inhibitor, were grown and imaged on such patterns for 36 h (Videos S5 and S6). CaMKK2-inhibited cells lost their junctional integrity and eventually started to grow on top of one another, suggesting that protrusive activity alone was not responsible for the loss of epithelial integrity. Moreover, MCF10A monolayers in which either CaMKK2 or AMPK was depleted by RNAi also began to lose epithelial cell-cell junctions and adopt a mesenchymal-like phenotype (Figures S7A and S7B).

We next examined whether the adoption of mesenchymal phenotype induced by AMPK inhibition could be due to the redistribution of junctional proteins. Both E-cadherin and ZO-1 began to lose their junctional localization pattern upon decreased AMPK activity, and E-cadherin accumulated in the cytoplasm (Figure S7C; Video S7). The loss of E-cadherin from cell-cell junctions was also associated with increased E-cadherin dynamics as measured from CaMKK2-inhibited MDCK monolayers by FRAP (Figures S7D and S7E). Thus, depletion of the immobile E-cadherin fraction from the AJs and loss of ZO-1 from TJs upon CaMKK2/AMPK inhibition may also contribute to the loss of epithelial integrity.

To further assess the effects of CaMKK2/AMPK inhibition on epithelial identity, we examined certain EMT markers in the inhibitor-treated cell cultures. Immunofluorescence microscopy and western blot experiments on MDCK cells, treated with either CaMKK2 or AMPK inhibitors, revealed elevation of vimentin expression that correlated with the altered cell morphology in the drug-treated monolayers (Figures 6A and 6B). Additionally, elevation of N-cadherin and Slug levels were detected from cell lysates, while beta-catenin levels remained unchanged (Figure 6C).

Because inactivation of CaMKK2 or AMPK led to a loss of epithelial integrity and upregulation of EMT-linked factors, we finally assessed whether disruption of the CaMKK2/AMPK pathway would affect the morphology of epithelial spheroids in a 3D environment. MCF10A cells typically form round, symmetrical, hollow-lumened structures in 3D Matrigel (Figure 6D, left image). Importantly, depletion of CaMKK2 or AMPK by small interfering RNA (siRNA) led to expansion of the 3D structures and appearance of abnormal protrusions (Figure 6D). Moreover, treatment of MCF10A cells with CaMKK2 or AMPK inhibitors led to abnormal 3D mammo sphere morphology and increase in the spheroid area (Figures 6E and 6F). Together, these results provide evidence that the CaMKK2/AMPK pathway can regulate the switch between mesenchymal and apicobasal phenotype through reorganization of the actin cytoskeleton and that the inhibition of this pathway therefore triggers loss of normal mammary epithelial structures in a 3D environment.

DISCUSSION

Epithelial morphology is maintained by adhesive cell-cell contacts, which are supported by peripheral actomyosin bundles. Mature AJs are dynamic, and their composition and strength vary as both E-cadherin and the associated actin-based structures are targeted by many biochemical signaling pathways that regulate tissue homeostasis in response to various external cues and forces (Priya and Yap, 2015). Here we show that contractile, epithelia-integrating peripheral actomyosin bundles can be derived from the pre-existing actin stress fiber precursor network and that their maintenance is dependent on the mechanosensitive CaMKK2/AMPK signaling pathway. Compromising the CaMKK2/AMPK signaling pathway led to a loss of these tension-maintaining peripheral actomyosin bundles and re-synthesis of actin stress fiber precursors. This was accompanied by the upregulation of EMT markers and loss of epithelial identity (Figure 7).

Actin at cell-cell junctions is composed of two dynamically and functionally distinct actin populations: junctional actin and thin peripheral actomyosin bundles (reviewed by Gomez et al., 2011; Takeichi, 2014; Braga, 2016). Interestingly, the assembly of peripheral actomyosin bundles from stress fiber precursors, transverse arcs, resembled the mechanism by which contractile ventral stress fibers are assembled in individually migrating mesenchymal cells: migrating mesenchymal cells typically display three types of actin stress fibers: dorsal stress fibers, transverse arcs, and ventral stress fibers (Hotulainen and Lappalainen, 2006). Of these, dorsal stress fibers and transverse arcs act as precursors structures for the mature contractile actomyosin bundles, ventral stress fibers (Hotulainen and Lappalainen, 2006; Tojkander et al., 2015). Also, single epithelial cells displayed the three categories of stress fibers, and they exhibited similar dynamic behavior compared with those of migrating mesenchymal cells (Video S1). Importantly, increasing confluency was accompanied by restricted retrograde flow of transverse arcs, resulting in lateral fusion of these actomyosin bundles at the periphery of the cells and consequent formation of peripheral actomyosin bundles (Figure 1; Figure S1). Similar packing of thin actin bundles was described by Zhang et al.

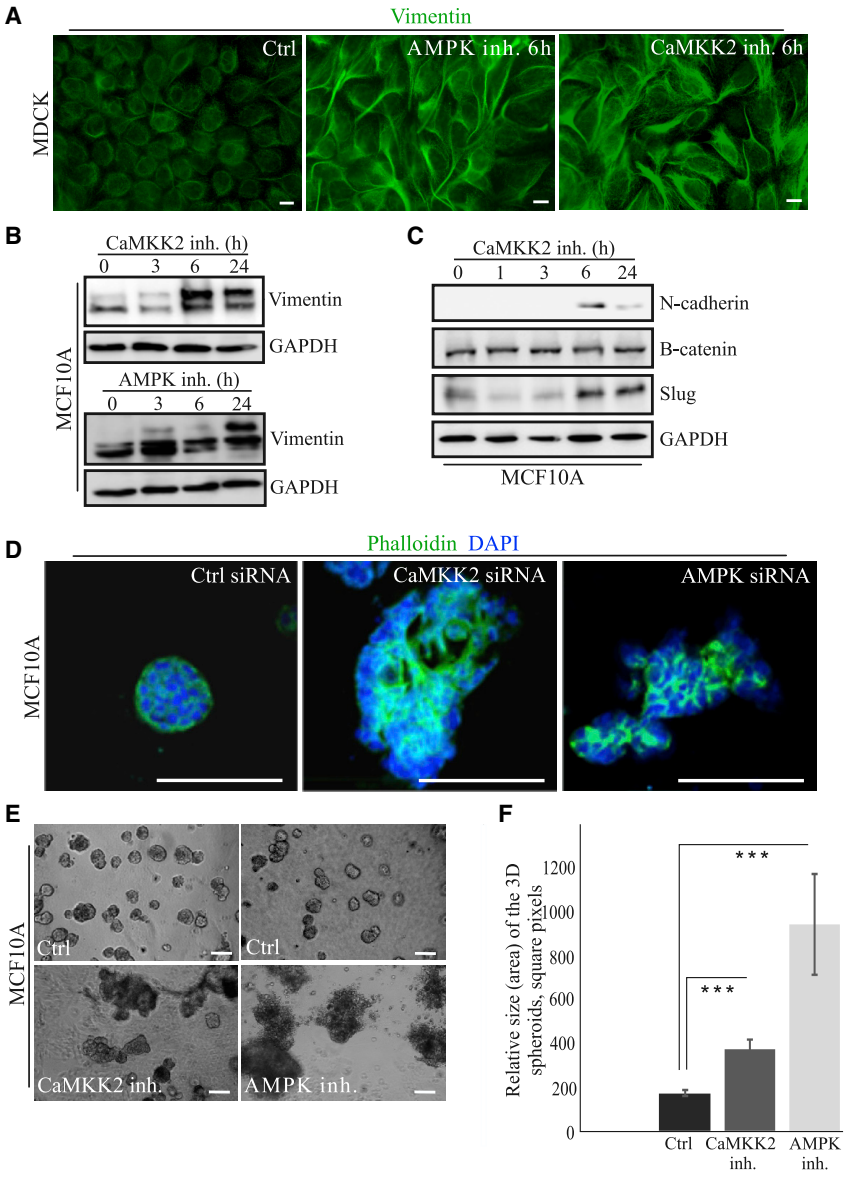

Figure 6. Inactivation of CaMKK2/AMPK Pathway in Epithelial Cultures Leads to Increased Expression of EMT-Linked Markers and Loss of Normal 3D Morphology

(A) MDCK cells were treated with AMPK or CaMKK2 inhibitor (5 μM compound c and 5 μM STO-609, respectively) for 6 h. Immunofluorescence staining showed changes in cell morphology and gradually elevated levels of endogenous vimentin (green) upon CaMKK2/AMPK inactivation. Specific antibody against vimentin was applied to visualize the intermediate filaments. Scale bars, 20 μm.

(B) Western blot analysis of lysates from CaMKK2- or AMPK-inhibited MCF10A cells at given time points revealed increased levels of vimentin protein upon inhibition of the CaMKK2/AMPK pathway. Note that upper band in the doublet of vimentin western blot corresponds to vimentin. GAPDH was used as a loading control.

(C) Western blot analysis of lysates CaMKK2-inhibited MCF10A cells revealed increased levels of N-cadherin and Slug after 6 h of CaMKK2 inhibition, while beta-catenin levels were unaltered. GAPDH was used as a loading control.

(D) Immunofluorescence images of MCF10A cells cultured in Matrigel for 14 days show that inhibition of the CaMKK2/AMPK pathway leads to a loss of normal 3D spheroid morphology. Control cells (left) formed typical round mammary spheroids with a hollow lumen, while cultures treated with CaMKK2 or AMPK siRNA had abnormal morphology with several cell protrusions to the 3D surroundings. Phalloidin was applied to visualize actin cytoskeleton (green) and DAPI the nuclei (blue). Scale bars, 100 μm.

(E) Bright-field images of MCF10A cells, cultured in 3D Matrigel. Control image shows cells after 5 days in culture, when typical 3D spheroid structures have formed. After formation of 3D mammary spheroids, cultures were treated with specific inhibitors against CaMKK2 and AMPK (15 μM STO-609, 15 μM compound c, respectively). Examples on 3D structures after 6 days with inhibitors are shown. Scale bars, 100 μm.

(F) Quantification of the 3D structures from control and CaMKK2 or AMPK inhibitor-treated cultures after 14 days. Mean ± SEM of the relative areas (square pixels) of spheroids is shown; n (ctrl) = 19, n (AMPK inhibited) = 19, and n (CaMKK2 inhibited) = 16 spheroids. ***$p < 0.001$ (Mann-Whitney-Wilcoxon rank-sum test).

(2005) prior to cell-cell contact formation in human keratinocytes, and the observed thin bundles most likely correspond to actin stress fiber precursors, transverse arcs. Besides that, the outer actomyosin cables of epithelial cell clusters matured through lateral packing of arcs, and the dynamics of these structures was similar to the dynamics of ventral stress fibers (Figures S1D and S3; Video S4). Although these epithelial cluster edges are compositionally distinct from cell-cell junctions, the maturation of actomyosin cables seems to follow similar mechanisms as the formation of peripheral actomyosin bundles. However, because junction formation and reorganization of the cytoskeletal structures along epithelial polarization is very complex, we cannot exclude other parallel mechanisms leading to the formation peripheral actomyosin bundles.

Assembly of peripheral actomyosin bundles in epithelial cultures was associated with an increase in the activity of AMPK and subsequent inhibitory phosphorylation of actin polymerization factor VASP (Figures 2A–2D). Because activation of AMPK and subsequent phosphorylation of its downstream target VASP on Ser239 residue was previously shown to affect actin polymerization activity of VASP (Benz et al., 2009) and consequently inhibit elongation of dorsal stress fibers in migrating osteosarcoma cells (Gateva et al., 2014; Tojkander et al., 2015), inhibition of dorsal stress fiber elongation could potentially

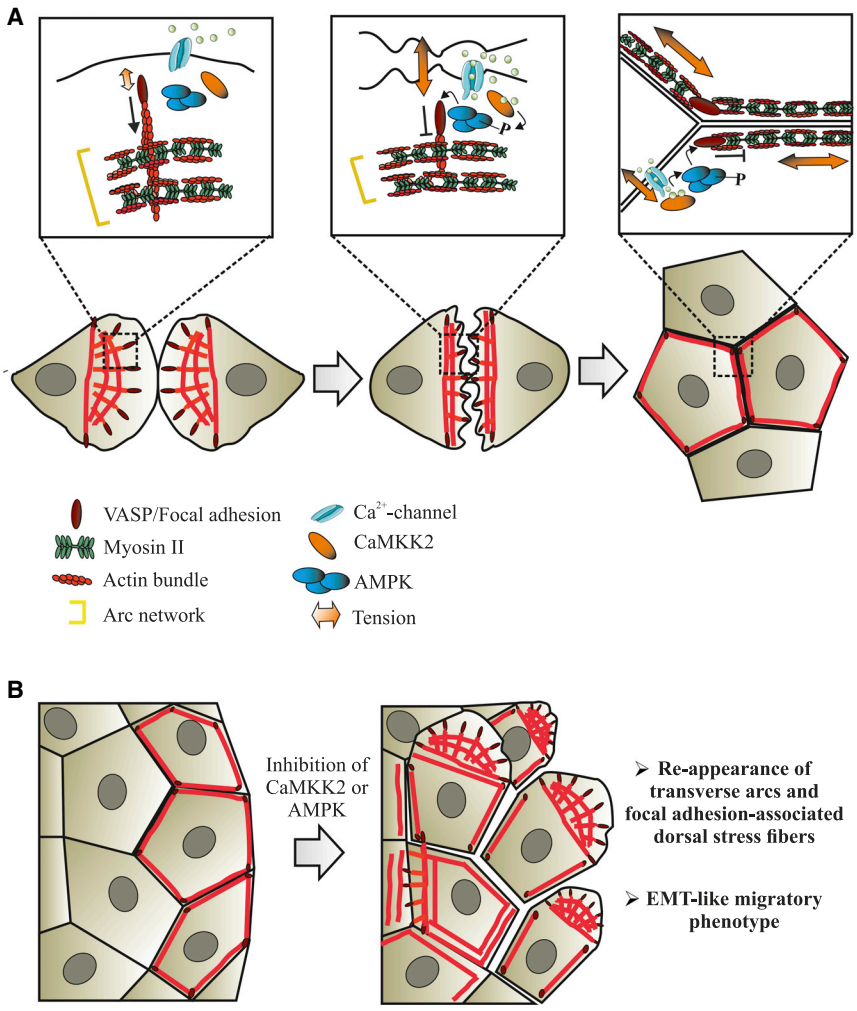

Figure 7. A Working Model for the Reorganization of Actin Stress Fibers upon Increasing Confluency

(A) Single migrating cells display actin stress fiber precursors, dorsal stress fibers, and transverse arcs at their leading edges. Dorsal stress fibers elongate from the focal adhesions through actin polymerization. Transverse arcs, which form parallel to the leading edge of the cell, flow toward the cell center with the elongating dorsal stress fibers. Elongation of dorsal stress fibers (black arrow) is at least partially dependent on a VASP-dependent mechanism. In single migrating cells, reorganization and lateral fusion of actin stress fiber precursors leads to the formation of ventral stress fibers toward the back of the cell. However, in more confluent cultures, cells start to feel the tension (orange arrows) from the neighboring cells. This triggers Ca^{2+}-dependent activation of the CaMKK2/AMPK pathway, which subsequently leads to inhibitory phosphorylation of VASP and halts growth of dorsal stress fibers from focal adhesions. This cascade further leads to fusion of transverse arcs at the edge of the cells, thereby contributing to the formation of peripheral actomyosin bundles. In confluent cultures, dorsal stress fiber elongation is blocked, and this maintains peripheral actomyosin bundles that are needed to support the tension at the cell-cell contacts.

(B) Inhibition of CaMKK2/AMPK pathway in confluent epithelial sheets leads to compromised cell-cell junctions and loss of outer actomyosin cables due to re-synthesis of the aforementioned actin stress fiber precursors and changes in epithelial force distribution. As a result, epithelial cells will adopt a mesenchymal cellular phenotype.

trigger the peripheral fusion of transverse arcs in confluent cultures. Further supporting the role of AMPK in regulating actin dynamics, we revealed that chemical induction of AMPK activity in single MCF7 cells was associated with the loss of dorsal stress fibers and formation of peripheral bundles, mimicking the peripheral actomyosin bundles of epithelial sheets. Although AMPK activity was clearly linked to the pSer239 phosphorylation on VASP, we cannot exclude the possibility that this phosphorylation of VASP would be indirect, catalyzed by another kinase.

Activation of AMPK was accompanied by an increase in cellular forces as measured by monolayer force microscopy. Moreover, AMPK activation led to increases in the levels of P-MLC and P-Vinc, which are indicative of elevated tension at the cell-cell contacts (Figure 5; Bays et al., 2014; Kassianidou et al., 2017; Subauste et al., 2004). These data suggest that AMPK dictates tension at cell-cell contacts through the regulation of peripheral actomyosin bundles. AMPK itself can be activated by several kinases, of which Lkb1 was for long considered the main upstream kinase. Lkb1-induced AMPK activity occurs mainly in metabolic stress, while other kinases are needed in response to different cellular stimuli (Hawley et al., 2003; Shaw et al., 2004; Hurley et al., 2005; Hardie and Lin, 2017). These other upstream kinases include CaMKK2, which in contrast to Lkb1 does not require decreased ATP/AMP ratio for activation but is triggered by elevated Ca^{2+} levels (Hong et al., 2005; Hurley et al., 2005; Woods et al., 2005). We found that the Ca^{2+}/CaMKK2 pathway is critical regulator of the AMPK-induced organization of epithelial actomyosin bundles. This is because inhibition of Ca^{2+} influxes or CaMKK2 led to the disruption of both peripheral actomyosin bundles and outer actomyosin cables and re-induced the elongation of dorsal stress fibers as well as resulted in the formation of lamellipodia-like protrusions at cell edges (Figures 3C–3G). In addition, studies by other groups have provided evidence that AMPK can be induced during the formation of cell-cell junctions in a Ca^{2+}-dependent manner (Zhang et al., 2006; Zheng and Cantley, 2007). We thus propose that tension from neighboring cells can trigger mechanosensitive ion channels that activate the CaMKK2/AMPK/VASP pathway and hence ensure the formation and maintenance of peripheral actomyosin bundles. Consequently, inactivation of this pathway leads to re-synthesis of dorsal stress fibers that force the flow of thin arc-like structures toward the cell center and thus compromise the

structure of thick peripheral actomyosin bundles (Figure 7). Undoubtedly, also other major pathways, such as Rac1/Arp2/3 and Rho/ROCK, are crucial for the formation of AJs (Noren et al., 2001; Kovacs et al., 2002; Lambert et al., 2002; Yamada and Nelson, 2007; Kalaji et al., 2012; reviewed by Lecuit and Yap, 2015) and manipulation of CaMKK2/AMPK pathway does not seem to regulate at least the activities of RhoA, Rac1, or cdc42 (Figures S2D and S2E).

Our results suggest that physical forces, induced by the increasing confluency, can trigger the activation of AMPK in epithelial cells. In support of this hypothesis, our experiments revealed that phosphorylation of AMPK's downstream target VASP at Ser239 residue was diminished when confluent MCF10A epithelial cultures were relaxed by blebbistatin treatment. Moreover, Bays et al. (2017) reported that AMPK is recruited to an E-cadherin mechanotransduction complex in a tension-sensitive manner, supporting the idea of tension-sensitive activation of AMPK at the cell-cell junctions.

Our results also revealed that inhibition of the mechanosensitive Ca^{2+}/CaMKK2/AMPK/VASP pathway in epithelial cultures results in redistribution of cellular forces through formation several new adhesions and appearance of lamellipodia-like protrusions (Figures 4 and S3). Although an increase in tractions at the edges of epithelial cell clusters was detected, the total cell-exerted forces, as measured from monolayers or cell doublets, were decreased upon inhibition of this pathway. This is most likely due to the lack of mature force-producing actomyosin bundles. Moreover, inhibition of either CaMKK2 or AMPK led to decreased junctional tension (Figures 4A, 4B, 4G, and 4H; see also Subauste et al., 2004; Bays et al., 2014; Kassianidou et al., 2017). This redistribution of cellular forces upon CaMKK2/AMPK inhibition could directly affect the epithelial integrity or alter E-cadherin dynamics, which are dependent on myosin II-mediated tension (see Shewan et al., 2005; Miyake et al., 2006; Engl et al., 2014). Recently, the NMIIA-containing actomyosin bundles were also found to be essential for the generation and maintenance of E-cadherin-based adhesions at cell-cell contacts (Heuzé et al., 2019). Additionally, appearance of dorsal stress fiber-like structures together with lamellipodial protrusions can result in disruption of cell-cell junctions, as protrusive activity was shown to induce epithelial scattering (Maruthamuthu and Gardel, 2014). It is thus possible that the CaMKK2/AMPK pathway ensures epithelial integrity through several overlapping mechanisms: by affecting the maturation of tension-providing actomyosin bundles and by directly regulating various proteins at adherens and TJs. Tension from the neighboring cells upon increasing confluency could thus activate these parallel pathways through induction of Ca^{2+}/CaMKK2/AMPK pathway.

Interestingly, inhibition of the Ca^{2+}/CaMKK2/AMPK pathway in epithelial cells led to an EMT-like phenotype and induced loss of normal 3D mammo sphere morphology (Figure 6). However, we cannot exclude the possibility that CaMKK2/AMPK pathway would directly regulate some EMT-linked factors that would then subsequently regulate the actin cytoskeleton. These findings on the connection of CaMKK2/AMPK pathway to EMT can also provide an explanation for the roles of AMPK and mechanosensitive Ca^{2+} channels in cancer progression (Carling, 2017; Fels et al., 2018). Disruption of junctional integrity due to compromised AMPK activity could also provide cells proliferative advantage through the loss of contact inhibition (Liang and Mills, 2013; Zadra et al., 2015). Although downregulation of AMPK has a clear link to cancer progression, immunohistological studies have revealed heterogeneous AMPK activity in different tumor types, and the consequences of the altered AMPK activity seem to be dependent on the biological background of the tumor (Liang and Mills, 2013; Zadra et al., 2015). Loss of AMPK expression is, however, rare, and cancer-associated changes in AMPK activity occur mostly because of its abnormal regulation.

Collectively, we have revealed that the CaMKK2/AMPK signaling pathway has an important role in reinforcing peripheral actomyosin bundles and maintaining epithelial integrity. These findings also provide a mechanistic explanation for earlier studies linking CaMKK2 and AMPK in junctional integrity and cancer progression (Peng et al., 2009; Aznar et al., 2016; Wang et al., 2016; Rowart et al., 2017, 2018). Although the tumor suppressive functions of AMPK have previously been suggested to be mediated through Lkb1 (Woods et al., 2003; Shaw et al., 2004), in the future it will be also important to investigate the role of the Ca^{2+}/CaMKK2 pathway in the context of AMPK and cancer invasion. Moreover, because AMPK can be either down- or upregulated in different cancers, it will be interesting to explore how different activity levels of AMPK affect junctional tension and scattering of various cancer cells.

STAR★METHODS

Detailed methods are provided in the online version of this paper and include the following:

- KEY RESOURCES TABLE
- LEAD CONTACT AND MATERIALS AVAILABILITY
- EXPERIMENTAL MODEL AND SUBJECT DETAILS
  - Cells
- METHOD DETAILS
  - Immunofluorescence microscopy
  - Structured Illumination Microscopy
  - Micropatterning
  - Western blotting
  - Traction force microscopy
  - Live cell imaging
  - AMPK biosensor studies
  - Rho GTPase kinase assay
  - 3D spheroid cultures
  - Monolayer analyses
- QUANTIFICATION AND STATISTICAL ANALYSIS
- DATA AND CODE AVAILABILITY

SUPPLEMENTAL INFORMATION

Supplemental Information can be found online at https://doi.org/10.1016/j.celrep.2020.02.096.

ACKNOWLEDGMENTS

The LMU imaging unit, at the Institute of Biotechnology, is acknowledged for their help in live-cell imaging experiments and data analyses. This work was supported by grants from the Academy of Finland, the Sigrid Juselius

Foundation, and the Jane and Aatos Erkko Foundation (S.T. and P.L.) and Cancer Society of Finland (P.L.).

AUTHOR CONTRIBUTIONS

E.K.R. performed the majority of the experiments and participated in writing the paper. J.I.L. performed all imaging experiments and figure generation for Figures 1 and S1 and participated in writing the paper. A.A. performed part of the monolayer force imaging experiments, inhibitor treatments, and analyses of the monolayer data. R.K. helped with traction force imaging experiments and analyses of intercellular forces together with N.S. P.L. participated in writing the manuscript. S.T. designed the experiments, performed traction force imaging, conducted statistical analyses, and wrote the paper.

DECLARATION OF INTERESTS

The authors declare no competing interests.

Received: April 10, 2019
Revised: December 2, 2019
Accepted: December 26, 2019
Published: March 24, 2020

REFERENCES

Abbott, M.J., Edelman, A.M., and Turcotte, L.P. (2009). CaMKK is an upstream signal of AMP-activated protein kinase in regulation of substrate metabolism in contracting skeletal muscle. Am. J. Physiol. Regul. Integr. Comp. Physiol. *297*, R1724–R1732.

Acharya, B.R., Wu, S.K., Lieu, Z.Z., Parton, R.G., Grill, S.W., Bershadsky, A.D., Gomez, G.A., and Yap, A.S. (2017). Mammalian diaphanous 1 mediates a pathway for E-cadherin to stabilize epithelial barriers through junctional contractility. Cell Rep. *18*, 2854–2867.

Adams, C.L., and Nelson, W.J. (1998). Cytomechanics of cadherin-mediated cell-cell adhesion. Curr. Opin. Cell Biol. *10*, 572–577.

Adams, C.L., Chen, Y.T., Smith, S.J., and Nelson, W.J. (1998). Mechanisms of epithelial cell-cell adhesion and cell compaction revealed by high-resolution tracking of E-cadherin-green fluorescent protein. J. Cell Biol. *142*, 1105–1119.

Arnold, T.R., Stephenson, R.E., and Miller, A.L. (2017). Rho GTPases and actomyosin: partners in regulating epithelial cell-cell junction structure and function. Exp. Cell Res. *358*, 20–30.

Aznar, N., Patel, A., Rohena, C.C., Dunkel, Y., Joosen, L.P., Taupin, V., Kufareva, I., Farquhar, M.G., and Ghosh, P. (2016). AMP-activated protein kinase fortifies epithelial tight junctions during energetic stress via its effector GIV/Girdin. eLife *5*, 20795.

Bays, J.L., Peng, X., Tolbert, C.E., Guilluy, C., Angell, A.E., Pan, Y., Superfine, R., Burridge, K., and DeMali, K.A. (2014). Vinculin phosphorylation differentially regulates mechanotransduction at cell-cell and cell-matrix adhesions. J. Cell Biol. *205*, 251–263.

Bays, J.L., Campbell, H.K., Heidema, C., Sebbagh, M., and DeMali, K.A. (2017). Linking E-cadherin mechanotransduction to cell metabolism through force-mediated activation of AMPK. Nat. Cell Biol. *19*, 724–731.

Benz, P.M., Blume, C., Seifert, S., Wilhelm, S., Waschke, J., Schuh, K., Gertler, F., Münzel, T., and Renné, T. (2009). Differential VASP phosphorylation controls remodeling of the actin cytoskeleton. J. Cell Sci. *122*, 3954–3965.

Braga, V. (2016). Spatial integration of E-cadherin adhesion, signalling and the epithelial cytoskeleton. Curr. Opin. Cell Biol. *42*, 138–145.

Burnette, D.T., Manley, S., Sengupta, P., Sougrat, R., Davidson, M.W., Kachar, B., and Lippincott-Schwartz, J. (2011). A role for actin arcs in the leading-edge advance of migrating cells. Nat. Cell Biol. *13*, 371–381.

Burnette, D.T., Shao, L., Ott, C., Pasapera, A.M., Fischer, R.S., Baird, M.A., Der Loughian, C., Delanoe-Ayari, H., Paszek, M.J., Davidson, M.W., et al. (2014). A contractile and counterbalancing adhesion system controls the 3D shape of crawling cells. J. Cell Biol. *205*, 83–96.

Carling, D. (2017). AMPK signalling in health and disease. Curr. Opin. Cell Biol. *45*, 31–37.

Curran, S., Strandkvist, C., Bathmann, J., de Gennes, M., Kabla, A., Salbreux, G., and Baum, B. (2017). Myosin II controls junction fluctuations to guide epithelial tissue ordering. Dev. Cell *43*, 480–492.e6.

de Rooij, J. (2014). Cadherin adhesion controlled by cortical actin dynamics. Nat. Cell Biol. *16*, 508–510.

Engl, W., Arasi, B., Yap, L.L., Thiery, J.P., and Viasnoff, V. (2014). Actin dynamics modulate mechanosensitive immobilization of E-cadherin at adherens junctions. Nat. Cell Biol. *16*, 587–594.

Fels, B., Bulk, E., Pethő, Z., and Schwab, A. (2018). The role of TRP channels in the metastatic cascade. Pharmaceuticals (Basel) *11*, E48.

Feng, D., Notbohm, J., Benjamin, A., He, S., Wang, M., Ang, L.H., Bantawa, M., Bouzid, M., Del Gado, E., Krishnan, R., and Pollak, M.R. (2018). Disease-causing mutation in α-actinin-4 promotes podocyte detachment through maladaptation to periodic stretch. Proc. Natl. Acad. Sci. U S A *115*, 1517–1522.

Gateva, G., Tojkander, S., Koho, S., Carpen, O., and Lappalainen, P. (2014). Palladin promotes assembly of non-contractile dorsal stress fibers through VASP recruitment. J. Cell Sci. *127*, 1887–1898.

Gomez, G.A., McLachlan, R.W., and Yap, A.S. (2011). Productive tension: force-sensing and homeostasis of cell-cell junctions. Trends Cell Biol. *21*, 499–505.

Green, K.J., Getsios, S., Troyanovsky, S., and Godsel, L.M. (2010). Intercellular junction assembly, dynamics, and homeostasis. Cold Spring Harb. Perspect. Biol. *2*, a000125.

Hardie, D.G., and Lin, S.C. (2017). AMP-activated protein kinase—not just an energy sensor. F1000Res. *6*, 1724.

Hawley, S.A., Boudeau, J., Reid, J.L., Mustard, K.J., Udd, L., Mäkelä, T.P., Alessi, D.R., and Hardie, D.G. (2003). Complexes between the LKB1 tumor suppressor, STRAD alpha/beta and MO25 alpha/beta are upstream kinases in the AMP-activated protein kinase cascade. J. Biol. *2*, 28.

Helwani, F.M., Kovacs, E.M., Paterson, A.D., Verma, S., Ali, R.G., Fanning, A.S., Weed, S.A., and Yap, A.S. (2004). Cortactin is necessary for E-cadherin-mediated contact formation and actin reorganization. J. Cell Biol. *164*, 899–910.

Heuzé, M.L., Sankara Narayana, G.H.N., D'Alessandro, J., Cellerin, V., Dang, T., Williams, D.S., Van Hest, J.C., Marcq, P., Mège, R.M., and Ladoux, B. (2019). Myosin II isoforms play distinct roles in adherens junction biogenesis. eLife *8*, e46599.

Hong, S.P., Momcilovic, M., and Carlson, M. (2005). Function of mammalian LKB1 and Ca2+/calmodulin-dependent protein kinase kinase alpha as Snf1-activating kinases in yeast. J. Biol. Chem. *280*, 21804–21809.

Hotulainen, P., and Lappalainen, P. (2006). Stress fibers are generated by two distinct actin assembly mechanisms in motile cells. J. Cell Biol. *173*, 383–394.

Hurley, R.L., Anderson, K.A., Franzone, J.M., Kemp, B.E., Means, A.R., and Witters, L.A. (2005). The Ca2+/calmodulin-dependent protein kinase kinases are AMP-activated protein kinase kinases. J. Biol. Chem. *280*, 29060–29066.

Irie, K., Shimizu, K., Sakisaka, T., Ikeda, W., and Takai, Y. (2004). Roles and modes of action of nectins in cell-cell adhesion. Semin. Cell Dev. Biol. *15*, 643–656.

Jensen, T.E., Rose, A.J., Jørgensen, S.B., Brandt, N., Schjerling, P., Wojtaszewski, J.F., and Richter, E.A. (2007). Possible CaMKK-dependent regulation of AMPK phosphorylation and glucose uptake at the onset of mild tetanic skeletal muscle contraction. Am. J. Physiol. Endocrinol. Metab. *292*, E1308–E1317.

Jiu, Y., Kumari, R., Fenix, A.M., Schaible, N., Liu, X., Varjosalo, M., Krishnan, R., Burnette, D.T., and Lappalainen, P. (2019). Myosin-18B promotes the assembly of myosin II stacks for maturation of contractile actomyosin bundles. Curr. Biol. *29*, 81–92.e5.

Kalaji, R., Wheeler, A.P., Erasmus, J.C., Lee, S.Y., Endres, R.G., Cramer, L.P., and Braga, V.M. (2012). ROCK1 and ROCK2 regulate epithelial polarisation and geometric cell shape. Biol. Cell *104*, 435–451.

Kannan, N., and Tang, V.W. (2015). Synaptopodin couples epithelial contractility to α-actinin-4-dependent junction maturation. J. Cell Biol. *211*, 407–434.

Kassianidou, E., Hughes, J.H., and Kumar, S. (2017). Activation of ROCK and MLCK tunes regional stress fiber formation and mechanics via preferential myosin light chain phosphorylation. Mol. Biol. Cell *28*, 3832–3843.

Kobielak, A., Pasolli, H.A., and Fuchs, E. (2004). Mammalian formin-1 participates in adherens junctions and polymerization of linear actin cables. Nat. Cell Biol. *6*, 21–30.

Kovacs, E.M., Goodwin, M., Ali, R.G., Paterson, A.D., and Yap, A.S. (2002). Cadherin-directed actin assembly: E-cadherin physically associates with the Arp2/3 complex to direct actin assembly in nascent adhesive contacts. Curr. Biol. *12*, 379–382.

Kovacs, E.M., Verma, S., Ali, R.G., Ratheesh, A., Hamilton, N.A., Akhmanova, A., and Yap, A.S. (2011). N-WASP regulates the epithelial junctional actin cytoskeleton through a non-canonical post-nucleation pathway. Nat. Cell Biol. *13*, 934–943.

Kraus, F., Miron, E., Demmerle, J., Chitiashvili, T., Budco, A., Alle, Q., Matsuda, A., Leonhardt, H., Schermelleh, L., and Markaki, Y. (2017). Quantitative 3D structured illumination microscopy of nuclear structures. Nat. Protoc. *12*, 1011–1028.

Krishnan, R., Park, C.Y., Lin, Y.C., Mead, J., Jaspers, R.T., Trepat, X., Lenormand, G., Tambe, D., Smolensky, A.V., Knoll, A.H., et al. (2009). Reinforcement versus fluidization in cytoskeletal mechanoresponsiveness. PLoS One *4*, e5486.

Lambert, M., Choquet, D., and Mège, R.M. (2002). Dynamics of ligand-induced, Rac1-dependent anchoring of cadherins to the actin cytoskeleton. J. Cell Biol. *157*, 469–479.

Lecuit, T., and Yap, A.S. (2015). E-cadherin junctions as active mechanical integrators in tissue dynamics. Nat. Cell Biol. *17*, 533–539.

Lecuit, T., Lenne, P.F., and Munro, E. (2011). Force generation, transmission, and integration during cell and tissue morphogenesis. Annu. Rev. Cell Dev. Biol. *27*, 157–184.

Liang, J., and Mills, G.B. (2013). AMPK: a contextual oncogene or tumor suppressor? Cancer Res. *73*, 2929–2935.

Marchiando, A.M., Graham, W.V., and Turner, J.R. (2010). Epithelial barriers in homeostasis and disease. Annu. Rev. Pathol. *5*, 119–144.

Maruthamuthu, V., and Gardel, M.L. (2014). Protrusive activity guides changes in cell-cell tension during epithelial cell scattering. Biophys. J. *107*, 555–563.

Mason, F.M., Xie, S., Vasquez, C.G., Tworoger, M., and Martin, A.C. (2016). RhoA GTPase inhibition organizes contraction during epithelial morphogenesis. J. Cell Biol. *214*, 603–617.

Mège, R.M., Gavard, J., and Lambert, M. (2006). Regulation of cell-cell junctions by the cytoskeleton. Curr. Opin. Cell Biol. *18*, 541–548.

Meng, W., and Takeichi, M. (2009). Adherens junction: molecular architecture and regulation. Cold Spring Harb. Perspect. Biol. *1*, a002899.

Miyake, Y., Inoue, N., Nishimura, K., Kinoshita, N., Hosoya, H., and Yonemura, S. (2006). Actomyosin tension is required for correct recruitment of adherens junction components and zonula occludens formation. Exp. Cell Res. *312*, 1637–1650.

Noren, N.K., Niessen, C.M., Gumbiner, B.M., and Burridge, K. (2001). Cadherin engagement regulates Rho family GTPases. J. Biol. Chem. *276*, 33305–33308.

Oakes, P.W., Beckham, Y., Stricker, J., and Gardel, M.L. (2012). Tension is required but not sufficient for focal adhesion maturation without a stress fiber template. J. Cell Biol. *196*, 363–374.

Owaribe, K., Kodama, R., and Eguchi, G. (1981). Demonstration of contractility of circumferential actin bundles and its morphogenetic significance in pigmented epithelium in vitro and in vivo. J. Cell Biol. *90*, 507–514.

Owaribe, K., and Masuda, H. (1982). Isolation and characterization of circumferential microfilament bundles from retinal pigmented epithelial cells. J. Cell Biol. *95*, 310–315.

Peng, L., Li, Z.R., Green, R.S., Holzman, I.R., and Lin, J. (2009). Butyrate enhances the intestinal barrier by facilitating tight junction assembly via activation of AMP-activated protein kinase in Caco-2 cell monolayers. J. Nutr. *139*, 1619–1625.

Pollard, T.D., Blanchoin, L., and Mullins, R.D. (2000). Molecular mechanisms controlling actin filament dynamics in nonmuscle cells. Annu. Rev. Biophys. Biomol. Struct. *29*, 545–576.

Priya, R., and Yap, A.S. (2015). Active tension: the role of cadherin adhesion and signaling in generating junctional contractility. Curr. Top. Dev. Biol. *112*, 65–102.

Rowart, P., Erpicum, P., Krzesinski, J.M., Sebbagh, M., and Jouret, F. (2017). Mesenchymal stromal cells accelerate epithelial tight junction assembly via the AMP-activated protein kinase pathway, independently of liver kinase B1. Stem Cells Int. *2017*, 9717353.

Rowart, P., Wu, J., Caplan, M.J., and Jouret, F. (2018). Implications of AMPK in the formation of epithelial tight junctions. Int. J. Mol. Sci. *19*, E2040.

Sahai, E., and Marshall, C.J. (2002). ROCK and Dia have opposing effects on adherens junctions downstream of Rho. Nat. Cell Biol. *4*, 408–415.

Schevzov, G., Whittaker, S.P., Fath, T., Lin, J.J.C., and Gunning, P.W. (2011). Tropomyosin isoforms and reagents. Bioarchitecture *1*, 135–164.

Shaw, R.J., Kosmatka, M., Bardeesy, N., Hurley, R.L., Witters, L.A., DePinho, R.A., and Cantley, L.C. (2004). The tumor suppressor LKB1 kinase directly activates AMP-activated kinase and regulates apoptosis in response to energy stress. Proc. Natl. Acad. Sci. U S A *101*, 3329–3335.

Shewan, A.M., Maddugoda, M., Kraemer, A., Stehbens, S.J., Verma, S., Kovacs, E.M., and Yap, A.S. (2005). Myosin 2 is a key Rho kinase target necessary for the local concentration of E-cadherin at cell-cell contacts. Mol. Biol. Cell *16*, 4531–4542.

Small, J.V., Rottner, K., Kaverina, I., and Anderson, K.I. (1998). Assembling an actin cytoskeleton for cell attachment and movement. Biochim. Biophys. Acta *1404*, 271–281.

Soiné, J.R., Brand, C.A., Stricker, J., Oakes, P.W., Gardel, M.L., and Schwarz, U.S. (2015). Model-based traction force microscopy reveals differential tension in cellular actin bundles. PLoS Comput. Biol. *11*, e1004076.

Subauste, M.C., Pertz, O., Adamson, E.D., Turner, C.E., Junger, S., and Hahn, K.M. (2004). Vinculin modulation of paxillin-FAK interactions regulates ERK to control survival and motility. J. Cell Biol. *165*, 371–381.

Sugimoto, A., Miyazaki, A., Kawarabayashi, K., Shono, M., Akazawa, Y., Hasegawa, T., Ueda-Yamaguchi, K., Kitamura, T., Yoshizaki, K., Fukumoto, S., and Iwamoto, T. (2017). Piezo type mechanosensitive ion channel component 1 functions as a regulator of the cell fate determination of mesenchymal stem cells. Sci. Rep. *7*, 17696.

Takeichi, M. (2014). Dynamic contacts: rearranging adherens junctions to drive epithelial remodelling. Nat. Rev. Mol. Cell Biol. *15*, 397–410.

Tambe, D.T., Hardin, C.C., Angelini, T.E., Rajendran, K., Park, C.Y., Serra-Picamal, X., Zhou, E.H., Zaman, M.H., Butler, J.P., Weitz, D.A., et al. (2011). Collective cell guidance by cooperative intercellular forces. Nat. Mater. *10*, 469–475.

Tojkander, S., Gateva, G., Schevzov, G., Hotulainen, P., Naumanen, P., Martin, C., Gunning, P.W., and Lappalainen, P. (2011). A molecular pathway for myosin II recruitment to stress fibers. Curr. Biol. *21*, 539–550.

Tojkander, S., Gateva, G., and Lappalainen, P. (2012). Actin stress fibers—assembly, dynamics and biological roles. J. Cell Sci. *125*, 1855–1864.

Tee, Y.H., Shemesh, T., Thiagarajan, V., Hariadi, R.F., Anderson, K.L., Page, C., Volkmann, N., Hanein, D., Sivaramakrishnan, S., Kozlov, M.M., and Bershadsky, A.D. (2015). Cellular chirality arising from the self-organization of the actin cytoskeleton. Nat. Cell Biol. *17*, 445–457.

Tojkander, S., Ciuba, K., and Lappalainen, P. (2018). CaMKK2 Regulates Mechanosensitive Assembly of Contractile Actin Stress Fibers. Cell Rep. *24*, 11–19.

Tojkander, S., Gateva, G., Husain, A., Krishnan, R., and Lappalainen, P. (2015). Generation of contractile actomyosin bundles depends on mechanosensitive actin filament assembly and disassembly. eLife *4*, e06126.

Tolić-Nørrelykke, I.M., Butler, J.P., Chen, J., and Wang, N. (2002). Spatial and temporal traction response in human airway smooth muscle cells. Am. J. Physiol. Cell Physiol. *283*, C1254–C1266.

Tsou, P., Zheng, B., Hsu, C.H., Sasaki, A.T., and Cantley, L.C. (2011). A fluorescent reporter of AMPK activity and cellular energy stress. Cell Metab. *13*, 476–486.

Vaezi, A., Bauer, C., Vasioukhin, V., and Fuchs, E. (2002). Actin cable dynamics and Rho/Rock orchestrate a polarized cytoskeletal architecture in the early steps of assembling a stratified epithelium. Dev. Cell *3*, 367–381.

Vasioukhin, V., Bauer, C., Yin, M., and Fuchs, E. (2000). Directed actin polymerization is the driving force for epithelial cell-cell adhesion. Cell *100*, 209–219.

Vignaud, T., Ennomani, H., and Théry, M. (2014). Polyacrylamide hydrogel micropatterning. Methods Cell Biol. *120*, 93–116.

Wang, B., Wu, Z., Ji, Y., Sun, K., Dai, Z., and Wu, G. (2016). L-glutamine enhances tight junction integrity by activating CaMK kinase 2-AMP-activated protein kinase signaling in intestinal porcine epithelial cells. J. Nutr. *146*, 501–508.

Watanabe, N., Kato, T., Fujita, A., Ishizaki, T., and Narumiya, S. (1999). Cooperation between mDia1 and ROCK in Rho-induced actin reorganization. Nat. Cell Biol. *1*, 136–143.

Woods, A., Johnstone, S.R., Dickerson, K., Leiper, F.C., Fryer, L.G., Neumann, D., Schlattner, U., Wallimann, T., Carlson, M., and Carling, D. (2003). LKB1 is the upstream kinase in the AMP-activated protein kinase cascade. Curr. Biol. *13*, 2004–2008.

Woods, A., Dickerson, K., Heath, R., Hong, S.P., Momcilovic, M., Johnstone, S.R., Carlson, M., and Carling, D. (2005). Ca^{2+}/calmodulin-dependent protein kinase kinase-beta acts upstream of AMP-activated protein kinase in mammalian cells. Cell Metab. *2*, 21–33.

Wu, S.K., Gomez, G.A., Michael, M., Verma, S., Cox, H.L., Lefevre, J.G., Parton, R.G., Hamilton, N.A., Neufeld, Z., and Yap, A.S. (2014). Cortical F-actin stabilization generates apical-lateral patterns of junctional contractility that integrate cells into epithelia. Nat. Cell Biol. *16*, 167–178.

Yamada, S., and Nelson, W.J. (2007). Localized zones of Rho and Rac activities drive initiation and expansion of epithelial cell-cell adhesion. J. Cell Biol. *178*, 517–527.

Yamada, S., Pokutta, S., Drees, F., Weis, W.I., and Nelson, W.J. (2005). Deconstructing the cadherin-catenin-actin complex. Cell *123*, 889–901.

Yano, T., Kanoh, H., Tamura, A., and Tsukita, S. (2017). Apical cytoskeletons and junctional complexes as a combined system in epithelial cell sheets. Ann. N Y Acad. Sci. *1405*, 32–43.

Yap, A.S., Brieher, W.M., Pruschy, M., and Gumbiner, B.M. (1997). Lateral clustering of the adhesive ectodomain: a fundamental determinant of cadherin function. Curr. Biol. *7*, 308–315.

Zadra, G., Batista, J.L., and Loda, M. (2015). Dissecting the dual role of AMPK in cancer: from experimental to human studies. Mol. Cancer Res. *13*, 1059–1072.

Zhang, J., Betson, M., Erasmus, J., Zeikos, K., Bailly, M., Cramer, L.P., and Braga, V.M. (2005). Actin at cell-cell junctions is composed of two dynamic and functional populations. J. Cell Sci. *118*, 5549–5562.

Zhang, L., Li, J., Young, L.H., and Caplan, M.J. (2006). AMP-activated protein kinase regulates the assembly of epithelial tight junctions. Proc. Natl. Acad. Sci. U S A *103*, 17272–17277.

Zheng, B., and Cantley, L.C. (2007). Regulation of epithelial tight junction assembly and disassembly by AMP-activated protein kinase. Proc. Natl. Acad. Sci. U S A *104*, 819–822.

STAR★METHODS

KEY RESOURCES TABLE

REAGENT or RESOURCE	SOURCE	IDENTIFIER
Antibodies		
Mouse anti-LC24	Schevzov et al., 2011	N/A
Rabbit polyclonal anti-NM-IIA	BioLegend	Cat#909801; PMID:29316444
Mouse monoclonal anti-MLC	Sigma-Aldrich	Cat#M4401; RRID:AB_477192
Mouse monoclonal anti-P-Ser239-VASP (clone 16C2)	Millipore	Cat# 05-611; RRID:AB_309841
Rabbit monoclonal anti-P-Thr172-AMPK	Cell Signaling Technology	Cat#4188; RRID:AB_2169396
Rabbit polyclonal anti-VASP	Prestige Ab, Atlas Antibodies	HPA 005724; RRID:AB_1858721
Rabbit monoclonal anti-P-Ser18/Thr19-MLCII	Cell Signaling Technology	Cat#3674; RRID:AB_2147464
Rabbit monoclonal anti-E-cadherin	CST	Cat#3195S; RRID:AB_2291471
Rabbit monoclonal anti-Vimentin	CST	Cat#5741; RRID:AB_10695459
Mouse monoclonal anti-vinculin (clone hVin-1)	Sigma-Aldrich	Cat# V9264; RRID:AB_10603627
Rabbit polyclonal anti-AMPK	Sigma-Aldrich	Cat#SAB4502329; RRID:AB_10745752
Rabbit monoclonal anti-ZO-1	Cell Signaling Technology	Cat#8193; RRID:AB_10898025
Rabbit monoclonal anti-N-cadherin	Cell Signaling Technology	Cat#14215; RRID:AB_2798427
Rabbit monoclonal anti-β-catenin	Cell Signaling Technology	Cat#8480; RRID:AB_11127855
Rabbit monoclonal anti-slug	Cell Signaling Technology	Cat#9585; RRID:AB_2239535
Mouse monoclonal anti-GAPDH	Sigma-Aldrich	Cat#G8795; RRID:AB_1078991
Goat anti-mouse HRP-linked secondary antibody	BioRad	Cat#170-6516; RRID:AB_11125547
Goat anti-rabbit HRP-linked secondary antibody	BioRad	Cat#170-6515; RRID:AB_11125547
Chemicals, Peptides, and Recombinant Proteins		
STO-609	Sigma-Aldrich	Cat#S1318s
AICAR	Sigma-Aldrich	Cat#A9978
GsMTx-4	Abcam	Cat#ab141871
ECM Gel from Engelbreth-Holm-Swarm murine sarcoma	Sigma-Aldrich	Cat#E1270
Experimental Models: Cell Lines		
Dog: Madin Darby Canine Kidney epithelial cells (female), MDCKs, or stable GFP-Actin MDCKs	kind gift from Prof. J. Nelson, Stanford University	N/A
Lifeact-TagGFP2 expressing MDCK and Lifeact-mKate expressing MDCK	This paper	N/A
Human: MCF10A (female)	ATCC	ATCC® CRL-10317
Human: MCF7 (female)	ATCC	ATCC® HTB-22
Human: 184A1 (female)	ATCC	ATCC® CRL-8798
Oligonucleotides		
siRNA for CaMKK2	Dharmacon	J-004842-08-0002; J-004842-09-0002; J-004842-10-0002
siRNA for AMPK (PRKAA1)	Dharmacon	J-005027-06
Recombinant DNA		
Lifeact-TagGFP2	a kind gift from Emmanuel Lemichez lab	N/A
mKate1.31-Lifeact7	a gift from Michael Davidson; Addgene	#54668

(*Continued on next page*)

Continued

REAGENT or RESOURCE	SOURCE	IDENTIFIER
AMPKAR biosensor (original plasmid was modified by replacing the N- and C-terminal ECFP and Venus tags with GFP and mCherry, respectively.	a kind gift from Lewis Cantley; Addgene	#35097
Software and Algorithms		
Fourier Transform Traction Cytometry	Tolić-Nørrelykke et al., 2002; Krishnan et al., 2009	N/A
Fiji, ImageJ, Tissue Analyzer plugin	plugin by Aigouy Benoit	https://imagej.nih.gov/ij/ 1997-2019

LEAD CONTACT AND MATERIALS AVAILABILITY

Lifeact-TagGFP2 and Lifeact-mKate expressing MDCK cell lines were generated during this study. All materials and reagents are available upon request. Further information and requests for resources and reagents should be directed to and will be fulfilled by the Lead Contact, Sari Tojkander (sari.tojkander@helsinki.fi).

EXPERIMENTAL MODEL AND SUBJECT DETAILS

Cells

Madin Darby Canine Kidney epithelial cells (female), MDCKs, or stable GFP-Actin MDCKs (kind gift from Prof. J. Nelson, Stanford University) were cultured in MEM with 10% FBS and penicillin-streptomycin; Human breast epithelial cell lines (female), MCF10A, 184A1 and MCF7, were maintained DMEM/F12 media supplemented with 5% Horse Serum, 20 ng/ml EGF, 0,5 mg/ml Hydrocortisone, 100ng/ml Cholera toxin, Insulin 10 μg/ml and penicillin-streptomycin. Cells were maintained in an incubator with 5% CO2, at +37°C temperature and plated on dishes one day prior to experiments unless stated otherwise. Treatments of cell cultures: CaMKK2 inhibitor, STO-609 (in DMSO; Sigma-Aldrich) was used in a final concentration of 5 or 10 uM and incubated for 3-24 hours; AMPK activity was inhibited with compound C (Dorsomorphin dihydrochloride, in DMSO; Sigma-Aldrich), final concentration of 5 uM for 3-24 hours; AMPK was activated with 25 uM AICAR for 16 hours; GsMTx-4 (in H2O; Abcam) was used in a final concentration of 5 uM for 3-16 h; For Ca^{2+}-depletion cells were incubated in a Ca^{2+}-free media (Ca^{2+}-free DMEM, GIBCO) for 3-24 h; CaMKK2 ON-TARGETplus siRNAs, Targeted Region: Non-Coding, ORF, J-004842-08-0002, J-004842-09-0002 and J-004842-10-0002 (Dharmacon) and AMPK siRNA (J-005027-06) were transfected with Ribojuice siRNA transfection reagent (71115-3, Millipore) according to the manufactureŕs instructions and incubated for 4 days on 2D cultures prior to imaging, fixation or preparation of cell lysates. Control cells were always treated with the corresponding solvent alone. Lifeact-TagGFP2 and Lifeact-mKate expressing MDCK cell lines were generated via transient transfection of the respective plasmids (Lifeact-TagGFP2 was a kind gift from Emmanuel Lemichez lab and mKate1.31-Lifeact7 a gift from Michael Davidson; Addgene# 54668), followed by selection of stable transfectants with 400ug/ml Geneticin.

METHOD DETAILS

Immunofluorescence microscopy

Cells were cultured on glass (MDCK) or laminin-coated (MCF10A, 184A1, MCF7) coverslips, washed with PBS before fixation with 4% PFA. Fixed cells were permeabilized with 0.1% Triton X-100/TBS for 5′ and moved to 0.2% Dulbecco/BSA. All immunofluorescence stainings were performed as in Tojkander et al., 2015. The following primary antibodies were used in stainings: anti-NM-IIA('tail') (#909801, BioLegend), anti-MLC ('head') (#M4401, Sigma), anti-Tropomyosin 2.1/4.2 (LC24, a gift from Peter.Gunning), anti-P-Ser239-VASP (clone 16C2, Millipore); anti-FLAG (F1804, Sigma-Aldrich), anti-P-Thr172-AMPK (#4188, Cell Signaling Technology); anti-VASP (HPA 005724, Prestige Ab, Atlas Antibodies), anti-P-Ser18/Thr19-MLCII (#3674, Cell Signaling Technology); E-cadherin (#3195S, Cell Signaling Technology), anti-Vimentin (#5741, Cell Signaling Technology) and anti-vinculin antibody (1:50) (hVin-1, Sigma, Saint Louis, MO). The following secondary antibodies were used to detect the primary antibodies: Alexa Fluor α-rabbit 488 and α-mouse 568 (Life Technologies™). Actin cytoskeleton was detected with Alexa 488-, −568- and −647-Phalloidins in 1:200 dilution (Life Technologies™) and DNA with DAPI (Life Technologies™). DABCO/Mowiol was used in mounting. Images were acquired with Leica DM6000 upright fluorescence wide field microscope equipped with Hamamatsu Orca-Flash4.0 V2 sCMOS camera. Colocalizations and lineprofiles were analyzed with ImageJ.

Structured Illumination Microscopy

Structured illumination imaging was performed at RT, using GE Deltavision OMX SR (GE Healthcare), 60x Plan-Apo N/1.42 NA Oil objective with 1.516 refraction index immersion oil, a laser module equipped with 488,568 and 640nm diode lasers and three sCMOS

cameras with imaging array of 1024 × 1024, leading to a pixel size of 0.08 and 0.125 microns for x/y and z respectively. AquireSR 4.4 and SoftWorx 7.0 (GE Healthcare) were used for image acquisition and 3D-SI reconstruction respectively. For SIM, the samples were grown and processed on either laminin (Sigma L2020) or collagen (Sigma C4243)-coated high precision coverslips according to protocol by Kraus et al., 2017, using Prolong Glass (Thermo Fisher Scientific) as mountant.

Micropatterning

Round micropatterns (Ø 400 um) were performed as in Vignaud et al., 2014. Custom designed quartz photomasks (Compugraphics International Ltd, Glenrothes, UK) and Novascan 8'' UV Ozone System were utilized in patterning the 4 kPa polyacrylamide substrates and the substrates were coated with fibronectin (Sigma Aldrich).

Western blotting

Cells were washed with cold PBS and lysed in 1% Triton X-100/PBS with protease & phosphatase inhibitors (539131 and 539131, Calbiochem). Protein concentrations were measured with Qubit® Protein Assay Kit (ThermoFisher Scientific). 4x LSB-DTT sample loading buffer was added to lysates and samples were boiled for 5′ prior to loading in SDS-PAGE gels (Bio-Rad). Wet transfer (Bio-Rad) with Immobilon-P Membrane, PVDF filter (Millipore) was used for blotting. 5% BSA/ 5% milk were used for blocking for 1h. Following antibodies were used for detection of specific proteins: anti-P-thr172-AMPK (#4188, Cell Signaling Technology), anti-AMPK (SAB4502329, Sigma), anti-P-ser239-VASP (clone 16C2, Millipore), anti-CaMKK2 (SAB1302099 and HPA017389, Sigma-Aldrich), anti-VASP (HPA 005724, Prestige Ab, Atlas Antibodies), anti-E-cadherin (#3195S, Cell Signaling Technology), anti-P-Ser19-MLCII (#3675, Cell Signaling Technology), anti-Vinculin (phospho Y822) (ab200825, Abcam), anti-ZO-1 (#8193, Cell Signaling Technology), anti-Vimentin (#5741, Cell Signaling Technology), anti-N-cadherin (#14215, Cell Signaling Technology), anti-β-catenin (#8480, Cell Signaling Technology), anti-Slug (#9585, Cell Signaling Technology) and mouse anti-GAPDH (G8795, Sigma-Aldrich). Anti-mouse or –rabbit HRP-linked secondary antibodies (Cell Signaling Technology) in 1:3000 dilution and Western HRP substrate (Luminata^{TM}Crescendo, WBLUR0100, Millipore) were used for chemiluminescence detection of the protein bands.

Traction force microscopy

To measure cell-exerted traction forces, epithelial cells were plated on elastic collagen-1-coated polyacrylamide (PAA) gel substrates of known stiffness (Young's Modulus/elastic modulus = 4 kPa) and incubated for 2-4 h prior to imaging in single cell studies and o/n for monolayer force studies. Substrates were surface-coated with sulfate fluorescent microspheres (Invitrogen, diameter 200 nm) before coating with collagen-1. Single isolated cells together with the underlying microspheres were imaged at multiple locations with 3I Marianas imaging system containing a heated sample chamber (+37°C) and controlled CO_2 (3I intelligent Imaging Innovations, Germany). 63x/1.2 W C-Apochromat Corr WD = 0.28 M27 objective was used. Following live cell imaging, the cells were detached from the substrates with 10 x Trypsin (Lonza Group) and a second set of microsphere images were obtained in a cell-free configuration. These images served as reference images. Spatial maps of microsphere displacements were achieved by comparing the reference microsphere images to the experimental images. By knowing the cell-exerted displacement field, substrate stiffness (4 kPa), and a manual trace of the cell boundary, we could compute the cell-exerted traction fields by using Fourier Transform Traction Cytometry (Tolić-Nørrelykke et al., 2002; Krishnan et al., 2009). From the traction fields, root mean squared magnitudes were computed. For the measurement of intercellular stresses, we utilized LifeAct-mKate-expressing MDCK cell doublets. These assays were performed at 6,3 kPa PAA dishes, with an optical resolution of 63x and analyzed at a spatial resolution of ~1μm. Intercellular stresses were calculated from the tractions using the approach of monolayer stress microscopy (Tambe et al., 2011; Feng et al., 2018).

Live cell imaging

For live cell imaging experiments, cells were transfected on previous day and replated prior to imaging on glass-bottomed dishes (μ-Dish Ibidi, MatTek Corporation or CELLviewTM, Greiner bio-one). For GFP-actin-expressing MDCK cells, imaging dishes were coated with collagen (Sigma C4243). For Lifeact-MDCK cell lines laminin (Sigma L2020) coating and Phenol Red-free MEM with 25mM HEPES media was used and cells were plated with 1:1 ratio (TagGFP2: mKate1.31) onto the imaging dishes. Time-lapse image series were acquired using GE Deltavision Ultra (General Electrics, USA) using Olympus 60X/1.42, Plan Apo N with 1.522 refractive index immersion oil and PCO-edge sCMOS camera with imaging array of 1024 × 1024. This resulted in pixel size of 0.107 for x/y. 3μm stack with 200nm steps was obtained every 5 minutes with AcquireUltra 1.1.1 software.

Time-lapse image series for GFP-actin MDCK cells were obtained using Leica TCS SP8, equipped with Leica LAS X 3.5.0, LIS (Life Imaging Services) incubation system (THE Cube, The Box and The Brick) set at +37°C and 5% CO2, white light laser or argon laser with DD 488/561 beam splitter, PMT detectors and HC PL APO 63x/1.20 W motCORR CS2 objective. Alternatively, 3I Marianas imaging system (3I intelligent Imaging Innovations), with an inverted spinning disk confocal microscope Zeiss Axio Observer Z1 (Zeiss) and a Yokogawa CSU-X1 M1 confocal scanner was utilized. The system has appropriate filters, heated sample chamber (+37°C), and controlled CO2. A 63x/1.2 W C-Apochromat Corr WD = 0.28 M27 objective was used. SlideBook 5.0 software (3I intelligent Imaging Innovations) and sCMOS (Andor) Neo camera were used for the image acquirement and recording. In Ca^{2+}-imaging experiments, the total internal reflection fluorescence (TIRF) microscopy of the same 3I Marianas imaging setup was used. A 63x/1.46 Alpha Plan-Apochromat Oil Corr WD = 0.10 M27 objective together with chroma TIRF filter cubes, 488/561 TRF59904 were utilized in

the TIRF experiments. Analysis of time-lapse data was conducted with Fiji, ImageJ and Image Pro. For Videos S1 and S3, Microvolution Fiji plugin was used to deconvolve the time-lapse series.

AMPK biosensor studies

To study how increasing confluency alters AMPK activity in epithelial cells, we utilized a fluorescence lifetime imaging (FLIM) -based AMPK biosensor (AMPKAR) (Tsou et al., 2011). AMPKAR biosensor is designed to produce fluorescence resonance energy transfer (FRET) in response to phosphorylation of AMPK, which allows spatiotemporal detection of AMPK activity in cells. We modified the original AMPKAR biosensor (Ampkar was a gift from Lewis Cantley; Addgene, plasmid #35097) by replacing the N- and C-terminal ECFP and Venus tags with GFP and mCherry, respectively, to make this construct suitable for our imaging system. For the experiments, MDCK cells on a 35 mm plate format were transfected with GFP alone (ctrl) or AMPKAR using NanoJuice transfection reagent (#71900 Millipore). Live cells were imaged at +37°C under a CO_2 hood. Leica TCS SP5 Multiphoton microscopy with HCX APO L 63x/0,90 W (water, dipping) objective was used for imaging. The microscopy is equipped with SPAD detectors and photon counting system allowing fluorescence lifetime imaging. Lifetime images were recorded with 256x256 image format, using the scanning speed of 200 Hz until the brightest pixel had at least 1000 counts. The average lifetime of the GFP was calculated first by manually segmenting cells, and then fitting one exponential decay curve to the lifetime histograms.

Rho GTPase kinase assay

RhoGTPase kinase assay was performed according to manufacturer's instructions (RhoA/Rac1/Cdc42 Activation Assay Combo Kit, Cell Biolabs INC, STA-405). Briefly, MCF10A cells were cultured approximately to 80%–90% confluence. Cells were treated with either DMSO, CaMKK2- or AMPK inhibitor for 24 hours. Cells were lysed, proceeded to pulldown and immunoblotted according to manufacturer's instructions.

3D spheroid cultures

ECM gel from Engelbreth-Holm-Swarm murine sarcoma (Sigma #E1270) was prepared according to manufacturer's instructions. MCF10A cells were trypsinized and 5000 cells in F12 media were seeded on top of Matrigel-coated eight-chamber slides. Formation of spheroids were monitored approximately two weeks before fixation and the area was measured using ImageJ.

Monolayer analyses

Tissue Analyzer plugin (Tissue Analyzer v1.0, Copyright 2007-2015 by Aigouy Benoit) was used for Fiji-ImageJ 1.52p ((National Institutes of Health, Bethesda, MD, USA, https://imagej.nih.gov/ij/, 1997-2019) software to segment the monolayers to cells using the watershed algorithm. Then we measured the cell area and the cell-to-cell bond lengths. Briefly, we cropped same size areas from the monolayers and performed bond recognition using the Tissue Analyzer built-in function. Cell bonds are pixels shared by exactly two cells and their length is presented in μm. Bounds are defined by the two cells that share them and the increase in their length is a measure for cell elongation. Each image was inspected and small false-recognized bonds were removed manually. The analysis was finalized and cell bond and cell size (data not shown) parameters were scored in at least 100 cells per treatment.

QUANTIFICATION AND STATISTICAL ANALYSIS

The statistical differences in western blot analyses, where the control values were set to 1, were assessed using the paired t test in Microsoft Excel 2013. Statistical differences in traction force experiments, AMPKAR biosensor experiments, quantifications of cellular phenotype, number of dorsal stress fibers and diameter of 3D structures were assessed by the Mann–Whitney–Wilcoxon rank-sum test (MWW). The statistical parameters (number of experiments, replicates and SEM) are listed in the figure legends. Box charts were done with Origin 2018 program (Whisker range 5-95, showing outliers) and column charts were done with Microsoft Excel 2013. Scatterplot charts were done with GraphPad Prsim 4.03 (GraphPad, La Jolla, USA). The difference between the groups in the scatterplots was evaluated with One-way ANOVA, Tukey post-test.

DATA AND CODE AVAILABILITY

This study did not generate any unique datasets or code. All raw data is available on request.